

Article

Source Apportionment of Ambient Particulate Matter (PM) in Two Western African Urban Sites (Dakar in Senegal and Bamako in Mali)

Thierno Doumbia ^{1,*}, Catherine Lioussé ¹, Marie-Roumy Ouafou-Leumbe ², Seydi Ababacar Ndiaye ³, Eric Gardrat ¹, Corinne Galy-Lacaux ¹, Cyril Zouiten ⁴, Véronique Yoboué ⁵ and Claire Granier ^{1,6}

¹ Laboratoire d'Aérodologie (LAERO), University of Toulouse, CNRS/UPS, 31100 Toulouse, France

² Department of Earth Sciences, Faculty of Sciences, University of Douala, Douala P.O. Box 2701, Cameroun

³ Laboratoire de Physique de l'Atmosphère et de l'Océan-Simeon Fongang (LPAO-SF), University of Dakar, Dakar 10700, Senegal

⁴ Géosciences Environnement Toulouse (GET), University of Toulouse, 31400 Toulouse, France

⁵ Laboratoire des Sciences de la Matière, de l'Environnement et de l'énergie Solaire, Félix Houphouët-Boigny University, Abidjan P.O. Box BP V 34, Côte d'Ivoire

⁶ NOAA Chemical Sciences Laboratory/CIRES, University of Colorado, Boulder, CO 80305-3337, USA

* Correspondence: thiernodoumbia@yahoo.fr or thierno.doumbia@aero.obs-mip.fr; Tel.: +33-5-6133-2766

Abstract: Following population growth and rapid urbanization, West African cities have become major sources of anthropogenic pollution. Additionally, Saharan dust has had a significant impact, representing a potentially toxic mix of sources for the population. This study characterizes the atmospheric composition and its sources in two African capitals, Bamako, Mali and Dakar, Senegal. TSP, PM₁₀ and PM_{2.5} samples were collected during the dry season in 2009 when pollution levels were high: chemical analysis included organic carbon (OC), elemental carbon (EC), ions, and metals. PM_{2.5} and PM₁₀ concentrations were 5–10 times and 3–8 times higher, respectively, than the 2005 WHO 24 h standards. Using PCA and PMF methodologies, five sources were identified in each city. In Bamako, traffic (motor vehicles and resuspended road dust) was the prevailing source of PM_{2.5} and PM₁₀, accounting for 47% and 45%, respectively. Crustal dust was the second most important source (24–30%), followed by solid fuel combustion (16–13%) and secondary aerosols (10–16%). In Dakar, the following sources of PM_{2.5} and PM₁₀ are identified: traffic (49%), mineral dust (16–25%), sea salts (15–20%) and industries (10–11%). Our study provides crucial information about the historical change in source characteristics in these two African cities, which can help for future mitigation strategies.

Keywords: air quality; particulate matter; source receptor models; PCA; PMF; West Africa



Citation: Doumbia, T.; Lioussé, C.; Ouafou-Leumbe, M.-R.; Ndiaye, S.A.; Gardrat, E.; Galy-Lacaux, C.; Zouiten, C.; Yoboué, V.; Granier, C. Source Apportionment of Ambient Particulate Matter (PM) in Two Western African Urban Sites (Dakar in Senegal and Bamako in Mali). *Atmosphere* **2023**, *14*, 684. <https://doi.org/10.3390/atmos14040684>

Academic Editors: Elena Hristova, Manousos Ioannis Manousakas, Anikó Angyal and Maria Gini

Received: 9 March 2023

Revised: 30 March 2023

Accepted: 31 March 2023

Published: 5 April 2023



Copyright: © 2023 by the authors. Licensee MDPI, Basel, Switzerland. This article is an open access article distributed under the terms and conditions of the Creative Commons Attribution (CC BY) license (<https://creativecommons.org/licenses/by/4.0/>).

1. Introduction

The role of atmospheric aerosols in climate change has long been recognized through their interactions with solar radiation and influence on cloud formation. However, as reported in the IPCC reports [1], significant uncertainties about the effect of aerosols on climate persist. On the other hand, several epidemiological and toxicological studies have demonstrated the impact of particulate matter (PM) on human health [2–4]. Exposure to PM can adversely affect human health via inhalation according to their size and chemical composition, especially in urban environments. For example, aerosol particles with aerodynamic diameters of less than 2.5 μm (PM_{2.5}) are recognized as being more likely to cause toxicological effects due to their ability to easily penetrate into human lungs [5,6]. In 2010, ambient air pollution, primarily PM_{2.5}, was responsible for 3.3 million premature deaths worldwide [7]. The chemical composition of PM, such as organic compounds and metals, contributes to their high toxicity [8,9]. The study conducted in African urban areas by Val et al. [9] on the pro-inflammatory effect of different particle sizes (ultrafine,

fine, and coarse fractions) highlighted the role of ultrafine particles primarily from combustion sources. The identification and quantitative evaluation of the contributions of different aerosol sources is important for understanding their implications in health and environmental effects and for defining mitigation policies. In developed countries, source characterization of atmospheric pollution has been investigated for several years. This is not the case in developing countries with densely populated regions, such as the West African capitals, where very few studies have been conducted. This region is heavily influenced by Saharan dust aerosols, which contribute significantly to total aerosol loads, especially during the dry season, when north-easterly trade winds (Harmattan) are predominant [10–12]. Deboudt et al. [13] demonstrated that in February 2006, desert dust dominated the coarse fraction and organic matter was the major constituent of the fine particles obtained in Mbour, a coastal site in Senegal. In urban areas, a large proportion of atmospheric particles is attributable to anthropogenic sources such as traffic (vehicular, two-wheel two-strokes and resuspended road particles), biomass and residential combustion (wood, charcoal and fuel), waste burning, and industries [14–20]. Indeed, mechanical processes such as the resuspension of road particles remain a large source due to tire abrasion, brake wear and the high number of unpaved roads in West African cities. All of these emission sources combined result in West African PM pollution levels being comparable to those observed in European, Asian, and United States megacities, and well above the World Health Organization (WHO) guidelines [19,21]. Due to a lack of long-term PM concentration data, Doumbia et al. [19] estimated PM_{2.5} from a one-year measurement of black carbon in Dakar (Senegal) in 2008 and found an annual average PM_{2.5} concentration that was four times higher than the WHO recommendation of 10 µg/m³.

Consequently, rapid deterioration of air quality has now become a serious challenge for the majority of capital cities in West Africa: in order to define policies to reduce particulate matter pollution at the source level, there is an urgent need for a better quantification of the sources of this atmospheric pollution. Receptor-oriented source apportionment models are often used to identify the number of aerosol sources and to estimate their contributions to measured concentrations [22–24]. Principal component analysis (PCA) [25,26], edge analysis (UNMIX) [27], chemical mass balance (CMB) [28], and positive matrix factorization (PMF) [29] are some of the popular multivariate models for determining the number of sources and elemental relative contributions. Although UNMIX and CMB methods have similar goals to PMF, they operate in different ways, with UNMIX not always able to resolve as many source factors as PMF [30]. The user must provide source profiles for mass apportionment when using CMB. The comparison of these different approaches shows that higher measurement uncertainty requirements in PMF produce better results than the other two models [31]. In our study, PCA is performed in conjunction with PMF to investigate and quantify the aerosol sources in West Africa urban sites. These two statistic models are considered here due to their complementarity, accessibility and relatively easy use. The PCA approach requires minimal inputs from the characteristics of the different sources, with the aim of quantifying information both on source profiles and the magnitude of absolute concentrations. The PCA is used as an explanatory tool to identify major sources of air pollutants, whereas the PMF is used to quantify the contributions of identified sources to all measured pollutants. The PMF is a non-data-sensitive technique that can manage and resolve inhomogeneous datasets without any previous univariate analysis. It does not require knowing historical emission source profiles and introduces estimated errors associated with each measured component. We also used enrichment factor (EF) analyses in addition to PCA and PMF to categorize air pollution sources in our sites. EF compares the ratios for various elements in measured atmospheric concentrations to the corresponding ratios in geological material [28,32].

A dataset from POLCA (POLLution des Capitales Africaines: African Capital Pollution), a jointly program between African and French universities, is used in this study [9,19,33]. The goal was to characterize atmospheric particulate pollution and its health impact at traffic sites in Bamako (Mali) and Dakar (Senegal), to handle different specificities typical of

West African megacities. Indeed, the measurement sites differ in terms of vehicle fleet, fuel type, road quality, residential combustions, dust episodes, and biomass burning impacts. Additionally, to study the upper limit of air quality impacts, samples were collected during intensive campaigns occurring in the selected sites during the dry season (January 2009 in Bamako and December 2009 in Dakar). The dry season is a time period that is well known for exhibiting high levels of pollution in such areas. Samples were analyzed for a comprehensive description of the physico-chemical characteristics of the aerosols, as well as their relative contributions to the aerosol particles with aerodynamic diameters of less than $2.5\ \mu\text{m}$ ($\text{PM}_{2.5}$), aerosol particles with aerodynamic diameters of less than $10\ \mu\text{m}$ (PM_{10}), and total suspended particles (TSP).

The focus of this paper is on the characterization of aerosol chemical composition and quantification of urban sources in Bamako and Dakar using the PMF statistic model in association with PCA analysis. We describe the methodology in Section 2 and discuss the results in Section 3.

2. Materials and Methods

2.1. Description of Monitoring Sites

PM samples were collected during the dry season in Bamako (Mali) and Dakar (Senegal), two West African cities. Bamako, the largest city in Mali, is located on the Niger River in the southwestern part of the country (Figure 1) and had a population of approximately 1.8 million inhabitants during the campaign in 2009 (12.5% of the national population) [34]. Measurements were taken at a downtown crossroad ($12^{\circ}39'\ \text{N}$, $8^{\circ}04'\ \text{W}$) between 20 January and 1 February 2009; a dust event episode occurred between 22 January and 24 January 2009 (Figure 2). In Dakar, a coastal city in West Senegal (Figure 1) with a population of about 2.5 million people in 2009 (21% of the national population) [35], measurements were performed between 1 and 13 December 2009, near a busy crossroad ($14^{\circ}40'\ \text{N}$, $17^{\circ}25'\ \text{W}$). Because of their proximity to markets, both sampling sites are heavily influenced by intensive human activities, particularly road traffic, but they have different air quality characteristics.

2.2. PM Sample Collection

Daily 24 h integrated aerosol samples were collected by filtration at the two West African urban sites using automatic aerosol samplers designed and developed for the INDAAF (International Network to study Deposition and Atmospheric chemistry in Africa, <https://indaaf.obs-mip.fr/>, accessed on 20 February 2023) program [36]. This system was designed to collect samples simultaneously using six lines: each particle mode (total suspended particles (TSP), particulate matter with diameters less than $10\ \mu\text{m}$ (PM_{10}) and particulate matter with diameters less than $2.5\ \mu\text{m}$ ($\text{PM}_{2.5}$)) was sampled separately with an individual pump operated at a flow rate of $18 \pm 7\ \text{l}\cdot\text{min}^{-1}$.

2.3. Environmental Parameters

At each sampling site, an automated meteorological station collected wind speed and direction, temperature (T), and relative humidity (RH). The coefficients of light scattering (σ_{scat}) and aerosol absorption (σ_{abs}) were also measured using a nephelometer (520 nm wavelength, model M903, Ecotech) and aethalometers (model AE-42 with seven wavelengths (370 to 950 nm) and 880 nm wavelength, model AE-16, Magee Scientific), respectively. Figures 2 and 3 display the diurnal variations of all of these parameters for the duration of the campaigns. There are distinct diurnal patterns in σ_{scat} and σ_{abs} for both sites over the entire measurement period, with two daily peaks: a morning peak between 7 and 9 a.m. and an evening peak between 5 and 7 p.m., with a second evening peak at 9 p.m. in Bamako. This diurnal variability is primarily caused by traffic and the evolution of the boundary layer during the day [19,37], which is common in urban areas.

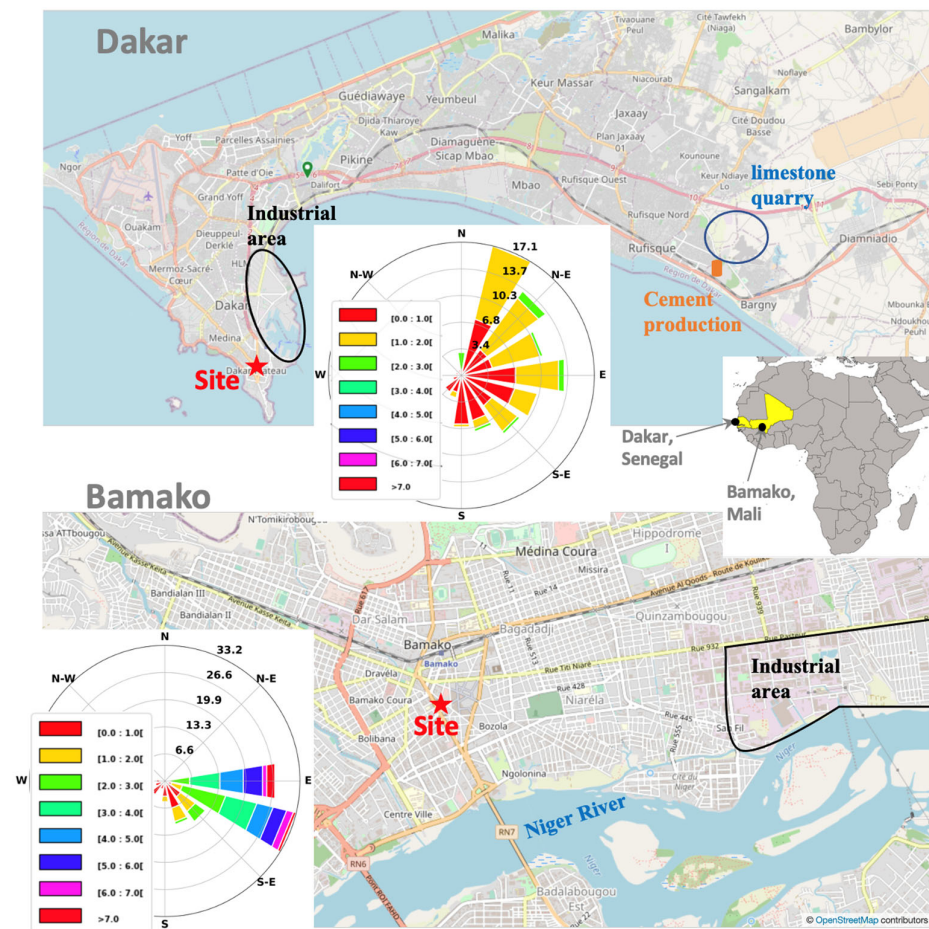


Figure 1. Map of measurement sites with superimposed wind roses during the two field campaigns in Dakar (top) and Bamako (down).

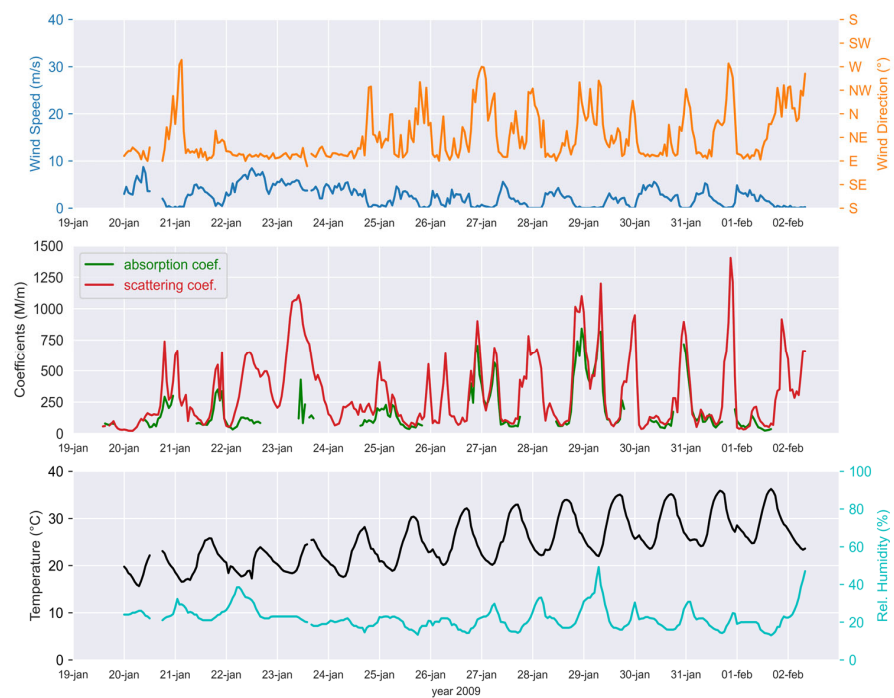


Figure 2. Light scattering and absorption coefficients, as well as meteorological data collected in Bamako during the dry season of 2009 (19 January to 2 February).

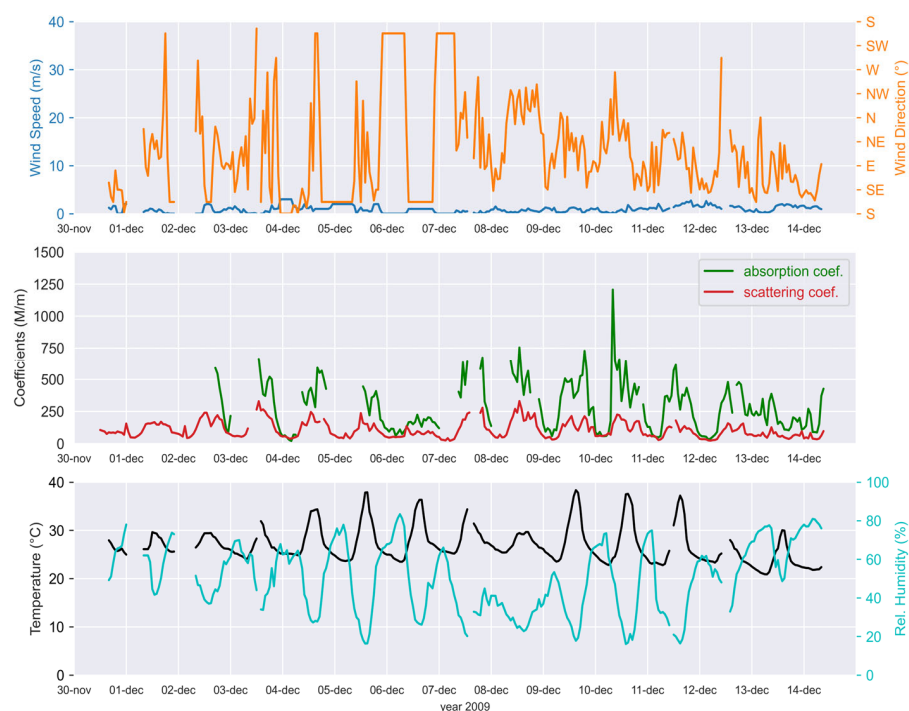


Figure 3. Light scattering and absorption coefficients, as well as meteorological data collected in Dakar during the dry season of 2009 (30 November to 14 December).

In Bamako (Figure 2), σ_{scat} and σ_{abs} generally show evening peaks (9 p.m.) more pronounced than in Dakar, coinciding with a thin boundary layer resulting from low ambient temperature and low westerly wind speed, except for the 22–23 January period, during which the diurnal variation was associated with high light scattering, low aerosol absorption, and high easterly wind speed ($8 \text{ m}\cdot\text{s}^{-1}$). The large difference observed between σ_{scat} and σ_{abs} was due to the dust episode that occurred on 22–23 January 2009.

In Dakar (Figure 3), σ_{scat} and σ_{abs} display large morning and evening peaks coinciding with morning and evening traffic peaks [19]. Lower values were observed late at night when traffic volume and air temperatures were low. Dakar had a lower σ_{scat} and a higher σ_{abs} than Bamako, indicating that the environmental characteristics of the two cities differed. To support this analysis, a σ_{abs} to σ_{scat} ratio was calculated and plotted for Bamako and Dakar to characterize traffic or dust influence [38] (Figure S1, Supplementary Materials). The mean ratio obtained in Dakar was 2.55 ± 0.99 , which was four times higher than the values obtained in Bamako (0.70 ± 0.33), indicating the importance of anthropogenic sources (e.g., traffic emissions) in Dakar, whereas the values in Bamako indicate an area influenced more by mixing air pollutant sources (combustion, dust and resuspended road particles).

2.4. Chemical Analyses

Aerosol particles were collected on 47 mm quartz filters for carbonaceous analyses and Teflon filters for water soluble ions and metal elements analyses. A calibrated microbalance (Model Mettler MC21S) was used to weigh Teflon filters before and after aerosol sampling for determining the PM gravimetric masses. The samples were conditioned for 24 h at a relative ambient humidity of $30 \pm 15\%$ prior to weighing and chemical analysis. TSP, PM_{10} and $\text{PM}_{2.5}$ were analyzed for carbonaceous elements (elemental carbon EC, organic carbon OC and total carbon TC), water-soluble inorganic compounds and metal elements. It should be noted that chemical analyses were performed a few days after sample collection.

- Water soluble inorganic compounds

Half of each Teflon filter was used in the analysis of inorganic ions (Na^+ , NH_4^+ , K^+ , Mg^{2+} , Ca^{2+} , SO_4^{2-} , NO_3^- , and Cl^-), using an ion chromatographic (IC) analyzer. These measurements

were conducted following the analytical protocol described in Adon et al. [39]. Briefly, cations were analyzed using Dionex ion chromatography (DX-100) and anions with a Dionex DX-500. Water extraction of the filter samples was performed by means of a 10 min long sonication in plastic vials with 30 mL of deionized ultra-pure water. All analyses were conducted immediately after extraction.

The quality control and quality assurance of the ion chemical analysis were ensured by measuring the blanks and the detection limit (DL), testing the reproducibility, and determining the measurement uncertainties. The DL is defined as three times the standard deviation (SD) of the procedure blank. The filter blank values and calculated DL for water soluble inorganic species are provided in Table S1 (Supplementary Materials). Only Mg^{2+} blank was lower than the DL, with a value of 1 ppb found in the 24 blanks tested.

The overall uncertainty of the measurements in this work was primarily due to three factors: sampling uncertainties, including possible gas–particle interactions and particle bounce-off; the relationship between the blank values, detection limits and concentrations measured; and random contamination issues. The uncertainty associated with each ion was calculated using Equation (1) from Alleman et al. [40]:

$$Unc = C \sqrt{u_r^2(m) + u_r^2(V) + \frac{u_c^2}{C^2}} \quad (1)$$

where C is the concentration of the element in the sample, $u_r(m)$ is the relative uncertainty of the mass m , $u_r(V)$ is the relative uncertainty of the air volume V , u_c is the absolute uncertainty due to the contamination. Using Equation (1), the estimated uncertainties were 4% for SO_4^{2-} , 18% for NH_4^+ , 44% for NO_3^- , 14% for Cl^- , 25% for Ca^{2+} , and 1% for Mg^{2+} and K^+ . NO_3^- concentrations have a high degree of uncertainty due to evaporation issues [41]. When NO_3^- was excluded, the average analytical uncertainty was estimated to be around 10%. A few NH_4^+ data were obtained in Bamako, most likely due to the same volatilization issue as with nitrate. As a result, NH_4^+ concentrations will not be shown here.

- Metal elements

The metal elements were determined by coupling microwave-assisted digestion with induced coupled plasma–mass spectrometry (ICP-MS). In this study, a special pre-treatment for loaded aerosols was set up following the Celio et al. [42] methodology. First, the samples, placed in 100 mL Teflon bombs, were subjected to microwave-assisted digestion within a mixture of ultra-high purity acids (10 mL 16N HNO_3 , 0.5 mL 28N HF). A closed-vessel microwave-assisted reaction system (MARS 5, CEM Corporation, Matthews, NC, USA) was used, with a two-step digestion program. During the first step, the temperature was ramped within 15 min to 160 °C. After a 10 min dwelling time, the temperature was ramped to 180 °C and samples were digested at this temperature for 30 min. The digested samples were then transferred to clean polypropylene tubes and diluted to 10 mL with HNO_3 0.37N. Samples were then analyzed using ultra-sensitive ICP-MS (7500ce Element Technologies).

The measurement quality of metal elements was ensured by controlling the blank and detection limit values. The concentrations of metals were determined in two types of blanks: vessel blanks (VB) and filter blanks (FB). The concentrations of trace metals in the vessel blank were used to evaluate the cleanliness of the microwave digestion and sample treatment processes. The VB was composed of acid solutions resembling those used in sample digestion. Metal concentrations in the FB were measured to establish a baseline from which field samples' element concentrations were subtracted. This was performed with VB and the same amount of filter paper that was used to collect aerosols in the field. The average concentrations in VB and FB, as well as the detection limits (DL), are shown in Table S2 (Supplementary Materials). The background concentrations of all elements were found to be higher in the filter blank than in the vessel blank. Most minor elements had DLs of less than 1 $\mu\text{g}\cdot\text{L}^{-1}$, whereas major elements (Ca, Na, K, Fe, Al, and Mg) had DLs ranging from 30 to 221 $\mu\text{g}\cdot\text{L}^{-1}$. Because our samples contain high concentration levels, the high sensitivity of the ICP-MS instrument accounts for the high

variability. The high DL values do not pose a problem for atmospheric samples, because the concentrations of these elements are typically much higher. Field blank values for elements such as Na, K, Mg, Fe, Al, Ti, Zn, Mn, Pb, Be, and Ni were slightly higher than filter blanks (Figure S2, Supplementary Materials), indicating a small field contamination of field blanks for these elements.

Standard reference materials (NIST SRM 1648 Urban Particulate Matter) prepared in the same manner as the digested samples, spikes, and duplicates were also analyzed to ensure the precision and accuracy of the analysis. Nine replicate NIST standard reference materials were measured. These materials were used directly without any treatment, except for acids added to match their matrix against samples analyzed in the same sequence. The reported recovery values for certified and non-certified elements are shown in Table S3 (Supplementary Materials). Except for Cr and Rb, which had recoveries of 60 and 69%, the digestion method provided good recoveries (84–105%, with a standard deviation (SD) range of 2.7–6.5%) for SRMs. Several authors reported comparable low Cr recovery percentages [43,44]. This could be due to the amount of HF used during mineralization, with more HF increasing recovery.

Over 40 elements were determined, with only some of them being retained for the sake of interpretation after subtraction of blank filter concentrations. Uncertainties associated with each element, as required by the PMF statistical model, were determined through the analysis of blank filters and the intercomparison of analytical techniques. The estimated uncertainties in Dakar were less than 15%, with the highest values for Ni and Pb, and did not exceed 20% in Bamako. These uncertainties are acceptable for use in source–receptor models such as positive matrix factorization (PMF).

Finally, the concentrations of calcium, potassium, sodium, and magnesium in PM_{2.5}, PM₁₀, and TSP measured by ICP-MS (inductively coupled plasma-mass spectrometry) and IC (ion chromatography) (see previous paragraph) were compared to ensure the quality of our data and to assess the ratio of soluble to non-soluble components. ICP-MS measures total elemental concentrations (Ca, K, Na, and Mg), whereas IC measures the water-soluble fraction (Ca²⁺, K⁺, Na²⁺, and Mg²⁺). Linear regressions for elements such as calcium and sodium showed slopes ranging from 0.9 to 1.3 in Dakar and from 1.9 to 2.1 in Bamako (Figure S3, Supplementary Materials), indicating that the majority of inorganic Ca and Na were soluble in Dakar (by 70–90%). Calcium and sodium concentrations measured by IC in Bamako were twice as low as those measured by ICP-MS, indicating that inorganic aerosols were less soluble in Bamako than in Dakar. This could be attributed to the strong influence of natural sources in Bamako, such as Sahara Desert dust and resuspended soil dusts by road traffic on unpaved roads. The total potassium (K) concentrations at both sites were approximately 3 to 4 times those of soluble potassium (K⁺), and this value reached 10 during the dust episode in Bamako. This is significant because soluble potassium (K⁺) is a key indicator for wood combustion [45]. The increasing K/K⁺ ratio during the dust event suggests that a fraction of the non-soluble potassium came from crustal dust. The same results were obtained for Mg/Mg²⁺ ratios (about 3–4). Mg²⁺ can be used as a tracer for marine aerosols. The increasing Mg/Mg²⁺ ratio (from 3 to 16) during the dust event suggests that some of the non-soluble magnesium is also derived from crustal material [46].

- Carbonaceous elements

Quartz filters used for carbonaceous analysis were preheated for 24 h at 600 °C to lower carbon blanks before being exposed. Twenty-four-hour samples (PM_{2.5}, PM₁₀ and TSP) were analyzed using a two-step combustion technique: total carbon (TC) and elemental carbon (EC) concentrations were determined using the THERMAL (carbon analyzer model G4 ICARUS CS TF, Bruker Axs, Germany) method developed by Cachier et al. [47] and the thermal-optical reflectance (TOR, Desert Research Institute analyzer) method following the IMPROVE temperature protocol [48], as indicated in Table S4 (Supplementary Materials). Organic carbon (OC) concentrations were finally calculated as the difference between TC and EC. In the THERMAL technique, carbonates were removed (decarbonated or decarbonation) under HCl fumes prior to analyses due to carbonates interfering with

carbon measurements. Sensitivity studies on the impact of decarbonation on Bamako and Dakar samples analyzed using TOR method were carried out. The decarbonation procedure is responsible for a decrease in the OC concentration (range 40–60%) and an increase in EC (range 10–23%), depending on the site and particle size fraction (Tables S5 and S6, Supplementary Materials).

For analysis, lower concentrations of species in aerosol samples necessitate low and stable blank values. The DL was calculated using the mean value of blanks and their standard deviation (SD). The blank value must be small because the magnitude of SD normally increases with the magnitude of the blank value. The quality control measurements on EC, OC and TC determinations performed at the Bamako and Dakar sites are summarized in Table S7 (Supplementary Materials). The average DRI instrument DL for TC, EC, and OC was 0.45, 0.13 and 0.33 $\mu\text{g}\cdot\text{cm}^{-2}$, respectively. These values are consistent with what the manufacturer reported. The obtained field blanks DL, on the other hand, were approximately 20 times higher for OC and 10 times higher for EC, indicating high field contamination.

Because different analytical methods can result in significant differences in OC and EC concentrations [49,50], an intercomparison of the THERMAL and TOR methods with no decarbonation was also performed as a data quality test. TC values obtained by the TOR method were close (difference less than 10%) to those obtained by the THERMAL method in both Bamako and Dakar samples, with a slope close to unity (Figure S4, Supplementary Materials). These findings corroborate those reported in the literature. When it comes to EC and OC, there are differences between the two methods. OC TOR was approximately 0.94 times the value of OC THERMAL in Dakar samples, compared to 0.85 in Bamako samples. This means that, despite differences in charring correction and temperature protocol in the TOR method, the two methods are comparable in terms of OC analysis. The analytical method used influences EC values, which may be due to variable source contributions. The EC concentrations determined by means of the TOR method were higher than the EC obtained using the THERMAL method. The EC TOR/EC THERMAL ratio in Dakar samples was 1.03, while it was 1.29 in Bamako samples. According to these findings, the differences between these two analytical methods are more pronounced in Bamako than in Dakar. This can be explained by three factors:

- The first factor is the presence of components such as brown carbon in carbonaceous aerosol [51], as brown carbon has the potential to influence splitting between OC and EC due to light absorption and medium thermal reactivity. Indeed, some brown carbon can be classified as OC, while the remainder is classified as EC [52]. Brown carbon was discovered to be emitted primarily by incomplete combustion, such as domestic fires, with this source heavily influencing the Bamako site [9]. Hitzenberger et al. [50] discovered comparable EC concentrations from diesel traffic sources using different methods. This finding is consistent with the fact that diesel emissions have a significant influence on Dakar samples (EC TOR to EC THERMAL ratio of 1.03 was found).
- The second factor is the mixing of aerosols. From Bamako, which is heavily influenced by dust, to Dakar, which is heavily influenced by traffic diesel, the EC TOR to EC THERMAL ratio decreases. The presence of dust particles in Bamako samples was assumed to interfere with thermal optical measurements, contributing to the observed large EC concentration variations.
- The third and final hypothesis is that the EC THERMAL is more sensitive to combustion aerosols originating from fossil fuels and biofuels [53], because these sources are more abundant in Bamako than in Dakar.

The estimated uncertainty was calculated using the following Equation (2) given by Chow et al. [54]:

$$Unc = \sqrt{(CV \times \overline{TC})^2 + DL^2} \quad (2)$$

where CV is the coefficient of variance for the replicate analysis, DL is the measured detection limit and \overline{TC} is the average filter blanks.

As part of the THERMAL method's quality control, filter blanks and instrument calibration were analyzed for two groups of samples: one for low carbon mass (<25 µgC) and one for high carbon level (>25 µgC). Before each analysis cycle, the instrument was calibrated by manually injecting sucrose into the analyzer. Table S7 (Supplementary Materials) shows good agreement between measured and target sucrose masses for both carbon calibrations, with a ratio close to unity indicating excellent instrument calibration. When compared to the DRI analyzer (TOR method), the carbon analyzer (THERMAL method) has lower detection limits. According to Equation (2), the uncertainty in measured TC using the TOR method was less than 10%. While the THERMAL method produced an uncertainty of 5%. The uncertainty in EC and OC varied by site and ranged from 5 to 30%. Based on all these results, the data measured using the THERMAL technique were considered in the following analysis.

2.5. Methods for Identifying and Quantifying Air Pollution Sources

2.5.1. Principal Component Analysis (PCA)

The PCA technique was used to identify potential sources of air pollution in Dakar and Bamako. The goal of PCA in this case was to reduce the number of variables to a smaller set of factors or sources while retaining as much information as possible from the original dataset [26]. This method helped to identify groups of correlated chemical compounds that come from the same air pollution sources. Due to the high variability of elemental concentrations, the chemical composition data were first transformed into a dimensionless standardized form. The new set of variables, known as principal components (PCs), were uncorrelated and ordered so that the first retained the majority of the variation present in all of the original variables. Assuming a linear relationship between observed variables (species concentrations) and a number of p principal components (sources), PCA is expressed in its simplified form as in Equation (3):

$$Z_{ij} = \sum_{k=1}^p g_{ik} \times h_{kj} \quad (3)$$

where Z_{ij} is the standardized concentration matrix, $k = 1, \dots, p$ is the number of principal components (sources), while g_{ik} is the factor loading matrix of correlations between compounds and PCs (sources) and h_{kj} is the matrix of factor scores.

To better identify groups of correlated compounds, the statistical method called "VARI-MAX rotation" was applied to the standardized concentration matrix to redistribute variances and provide a more interpretable structure to PCs (sources). After rotation, species from the same source were linked to the same PC with high weights (factor loadings), and this PC was then associated with a specific air pollution source before using PMF to quantify this source.

2.5.2. Positive Matrix Factorization (PMF)

Another statistical method, called positive matrix factorization (PMF version v5.0) was used to quantify the contribution of the various sources to the particulate matter emissions. The principles and usage of this approach are detailed in the EPA (Environment Protection Agency) PMF user guide (<https://www.epa.gov/air-research/epa-positive-matrix-factorization-50-fundamentals-and-user-guide>). This method involved a minimization of an objective cost function Q [29,55,56], given by Equation (4):

$$Q = \sum_{i=1}^n \sum_{j=1}^m \frac{e_{ij}^2}{s_{ij}^2} \quad (4)$$

where e_{ij} is the residual associated with i^{th} species concentrations measured in the j^{th} sample, s_{ij} is an uncertainty estimate for i^{th} species measured in the j^{th} sample, n and m are, respectively, the numbers of samples and of species.

PMF used both measured concentrations and uncertainty estimates to generate calculated chemical profiles and time series associated with each of the chemical profiles. The selection of species to be included in the analysis data depended on the goal of the study and on the quality of available species measurements. PMF analysis, like the PCA method, included the selection of 27 chemical variables (Al, Be, Ti, V, Mn, Co, Fe, Tl, K, As, Rb, Mg, Na, Ca, Ni, Se, Cr, Cu, Zn, Cd, Sb, EC, OC, Cl^- , SO_4^{2-} , and NO_3^-) that were detected in the 39 and 36 samples in Bamako and Dakar, respectively. It should be noted that total suspended particle (TSP) concentrations were included in the factor analysis in order to increase the robustness of the results. Receptor models do not generally provide strict guidelines regarding the minimal number of required samples. This is because the number of required samples also depends on the number of analyzed chemical species (source tracers in particular), the quality of the data and the number of contributing sources [57]. Moreover, it has been seen that the number of samples in the dataset employed in the published literature ranges from ten [58] to tens of thousands [59]. Following these results and due to the number of sources impacting our two sites, 39 and 36 samples were considered as a satisfactory number of observations to conduct PMF apportionment.

To assess the contribution of the identified factors to the collected data, the analysis included PM mass as an explicit species. In the species concentrations table, missing values were replaced with the median value of species with assigned uncertainty values multiplied by four times the standard deviation. Species with a percentage of missing data over 70% were excluded from the dataset, which was the case for Pb and NH_4^+ . The basic criterion retained for PCA and PMF was that aerosol concentrations must be greater than the detection limit (DL). When the measured concentrations were less than the DL, an adjustment was required; typically, data below the DL are rejected or replaced by $\text{DL}/2$, with an uncertainty of $5 \times \text{DL}/6$ [56]. This late methodology was applied here. Furthermore, a data quality classification based on the signal-to-noise ratio was implemented, indicating whether the variability in measurements is real or due to data noise. The species were classified as “strong” if the signal to noise ratio was greater than 2, “weak” if it was between 0.2 and 2, and “bad” if it was less than 0.2 [60]. We multiplied the concentration by 3 for “weak” data. Only PM mass and Sb were categorized as “weak” in our measurements. As a result, the EPA PMF user guide recommended setting an extra modeling uncertainty. It was set to 20% in this study.

Before applying the PMF, isolated events such as dust episodes were screened, as the contributions due to dust episodes could not be distinguished by the PMF technique [30]. The performance of the PMF model was assessed by comparing reconstructed daily mean PM concentrations from all sources to measured values for each species (Tables S8 and S9, Supplementary Materials). The largest uncertainties in Bamako (15% for Ni, 16% for EC and 14% for OC) and in Dakar (10% for PM) can be attributed to data quality because missing values in some of these variables (EC and OC) were replaced by their median values, and associated uncertainties were assigned to be four times the mean values. PM was included as a variable, with high uncertainty determined due to missing values [61]. However, with significant correlation coefficients, there was generally good agreement between measured and calculated concentrations, suggesting that the identified factors effectively reproduce measured masses.

3. Results and Discussion

3.1. Aerosol Chemical Mass Concentrations

Figure 4 shows time series of $\text{PM}_{2.5}$, PM_{10} , and TSP mass concentrations measured during POLCA's intensive campaigns in Bamako (20 January 2009–1 February 2009) and Dakar (1 December to 13 December 2009), as well as the 48 h back trajectory analysis from the Hybrid Single-Particle Lagrangian Integrated Trajectory (HYSPLIT) modeling system [62]. The concentration of $\text{PM}_{2.5}$, PM_{10} , and TSP in Bamako ranged from 131.6 to 1194.3 $\mu\text{g}\cdot\text{m}^{-3}$, 151.1 to 1513.1 $\mu\text{g}\cdot\text{m}^{-3}$ and 356.7 to 1768.9 $\mu\text{g}\cdot\text{m}^{-3}$, with average concentrations of 276.8, 503.6 and 705.3 $\mu\text{g}\cdot\text{m}^{-3}$, respectively. The extreme daily values were

measured on 22 January 2009 (Figure 4a): the HYSPLIT back trajectories suggest that these high values were caused by a Saharan dust event that occurred that day. According to Figure 4b, the air mass that was stagnating over Bamako at the beginning of the measurements (22–23 January) came from the southwest part of Algeria and had passed over the Great Western Erg. This dust episode had an impact on all PM modes. The average daily PM concentrations remained very high without the dust event ($583 \mu\text{g}\cdot\text{m}^{-3}$ for TSP, $390 \mu\text{g}\cdot\text{m}^{-3}$ for PM_{10} , and $219 \mu\text{g}\cdot\text{m}^{-3}$ for $\text{PM}_{2.5}$). In Dakar, the average daily concentrations ranged from 152 to $479 \mu\text{g}\cdot\text{m}^{-3}$ for TSP, 82 to $293 \mu\text{g}\cdot\text{m}^{-3}$ for PM_{10} , and 81 to $258 \mu\text{g}\cdot\text{m}^{-3}$ for $\text{PM}_{2.5}$, with average values of 274.9, 155.9 and $138.2 \mu\text{g}\cdot\text{m}^{-3}$, respectively. Both $\text{PM}_{2.5}$ and PM_{10} show peaks on December 3 and 10, corresponding to Thursdays, when activity at the Sandaga market, where the measuring instruments were located, is higher (Figure 4c). Only TSP shows a peak on December 8, which coincides with the origin of the air mass to the southeast (Figure 4d), implying a contribution from long-range transport in the high concentrations measured. This late hypothesis is in line with the observed dust episode. In addition, most air mass back trajectories had a continental origin, implying a potential mix of sources (dust, biomass burning, and anthropogenic) that may explain the high measured PM concentration during the measurement period (Figure 4d). Lower concentrations were measured in Dakar over the weekend of 12–13 December, when cleaner air masses passed over the Atlantic Ocean before arriving at the measurement site. The PM_{10} and $\text{PM}_{2.5}$ concentrations were up to twice and 3.4 times the Senegalese daily national standard of 150 and $75 \mu\text{g}\cdot\text{m}^{-3}$, respectively. These limit values are two to three times higher than the other international standards. Mali currently lacks a national air quality standard.

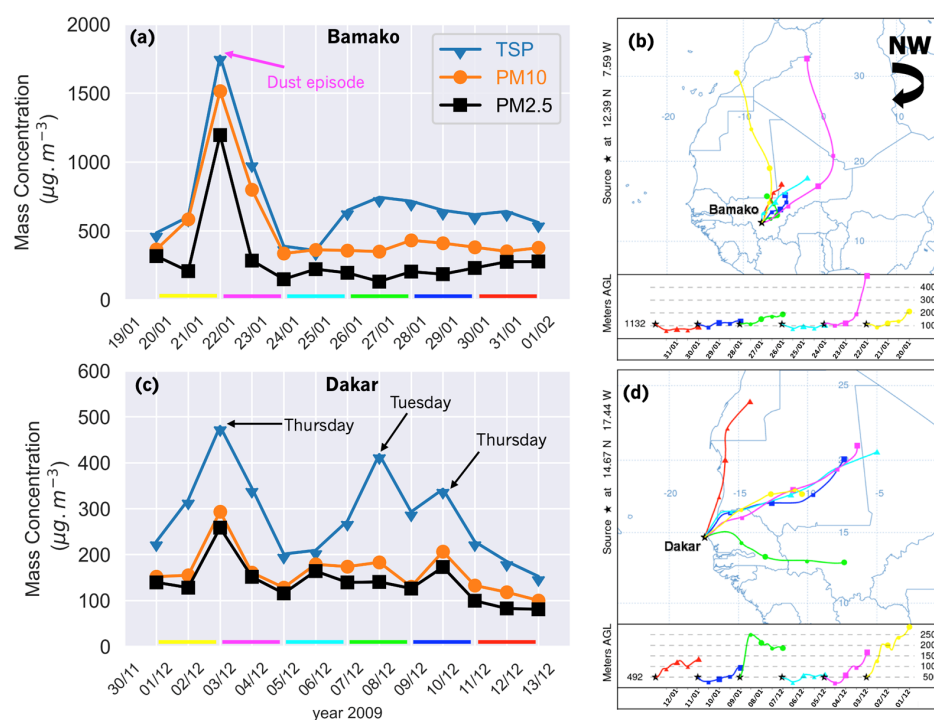


Figure 4. Map of the daily evolution of PM (TSP, PM_{10} , and $\text{PM}_{2.5}$) mass concentrations (a) in Bamako and (c) Dakar, as well as HYSPLIT 48 h air mass back trajectories arriving (b) in Bamako for the period from 20 January to 1 February 2009, and (d) in Dakar for the period from 1 to 13 December 2009. The individual 48 h back trajectories are represented by color lines.

In both Bamako (Pearson correlation coefficient $r = 0.89\text{--}0.94$) and Dakar ($r = 0.78\text{--}0.97$), the temporal evolutions of the three aerosol fractions show significant correlations between the different particle sizes, indicating that these aerosols share sources. The concentrations in both Dakar and Bamako (excluding dust episode) are comparable to those measured in Conakry (Guinea) during the Harmattan period (winds blowing northeast from January

to February) in 2004, namely 80–358 $\mu\text{g}\cdot\text{m}^{-3}$ for PM_{10} and 38–177 $\mu\text{g}\cdot\text{m}^{-3}$ for $\text{PM}_{2.5}$ [16]. Furthermore, the average $\text{PM}_{2.5}$ concentrations in our study are of the same order of magnitude as the average values of 141.3, 175.3, and 269.7 $\mu\text{g}\cdot\text{m}^{-3}$ obtained in a traffic and waste burning site in Abidjan, and traffic site in Cotonou in January 2016 and 2017 [63]. More recent measurements of $\text{PM}_{2.5}$ in Dakar show that, for the years 2018–2019, average daily concentrations ranged from 280.6 to 302.7 $\mu\text{g}\cdot\text{m}^{-3}$ [64], suggesting an increase in concentration over the previous ten years. This can be explained by rapid urbanization and population growth, as the population of Dakar increased by about 1 million residents between 2007 and 2017. According to these comparisons, the PM concentrations in Dakar and Bamako are typical of the urban pollution in western Africa.

Table 1 summarizes the statistics (arithmetic mean, standard deviation and percentage in total mass) of measured chemical composition mass concentration in Bamako and Dakar, while Figures S5 and S6 (Supplementary Materials) show the temporal evolution of OC, EC, ions and twenty-two metals measured in $\text{PM}_{2.5}$, PM_{10} , and TSP.

Table 1. Average 24 h concentrations (in $\mu\text{g}\cdot\text{m}^{-3}$) for TSP, PM_{10} , and $\text{PM}_{2.5}$ and associated elemental compositions in Bamako (including dust episode) and Dakar. Values in parentheses are percentages in total masses.

Species	Bamako			Dakar		
	TSP	PM10	PM2.5	TSP	PM10	PM2.5
Mass PM	705.3 ± 99.3	503.6 ± 112.4	276.8 ± 94.7	274.9 ± 27.43	155.9 ± 15.7	138.2 ± 12.7
Cl ⁻	3.43 (<1)	3.36 (<1)	2.12 (<1)	8.45 (3)	8.13 (5)	1.77 (1)
NO ₃ ⁻	1.87 (<1)	1.87 (<1)	1.18 (<1)	2.06 (<1)	2.31 (1)	0.97 (<1)
SO ₄ ²⁻	4.44 (<1)	4.29 (<1)	2.98 (1)	6.18 (2)	7.49 (5)	4.75 (3)
Na ⁺	2.21 (<1)	1.70 (<1)	1.02 (<1)	5.1 (2)	5.04 (3)	1.21 (<1)
K ⁺	3.5 (<1)	3.17 (<1)	2.02 (<1)	0.99 (<1)	0.99 (<1)	0.59 (<1)
Mg ²⁺	0.87 (<1)	0.75 (<1)	0.49 (<1)	0.72 (<1)	0.71 (<1)	0.28 (<1)
Ca ²⁺	7.14 (1)	7.09 (1)	5.29 (2)	12.17 (4)	13.65 (9)	11.43 (8)
Inorganic ions	24.06 (3)	22.99 (5)	15.69 (6)	36.09 (13)	38.95 (25)	21.50 (16)
EC	23.34 (3)	18.85 (4)	27.11 (10)	20.14 (7)	16.41 (11)	15.88 (11)
OC	102.4 (15)	82.38 (16)	102.4 (37)	69.19 (25)	34.92 (22)	35.83 (26)
TC	125.74 (18)	101.23 (20)	129.51 (47)	89.33 (32)	51.33 (33)	51.71 (37)
Al	21.23 (3)	22.24 (4)	17.98 (6)	9.66 (3)	7.07 (4)	4.11 (3)
Fe	21.91 (3)	20.41 (4)	14.28 (5)	9.00 (3)	5.54 (3)	3.49 (2)
Ti	2.35	2.14	1.47	0.89	0.54	0.34
Mn	0.35	0.32	0.22	0.15	0.11	0.06
Zn	0.18	0.15	0.12	0.21	0.16	0.11
Cr	0.10	0.09	0.06	0.04	0.02	0.02
V	0.06	0.05	0.04	0.07	0.07	0.05
Cu	0.03	0.04	0.02	0.08	0.19	0.13
Ni	0.02	0.02	0.03	0.03	0.03	0.03
Pb	0.02	0.02	0.04	0.03	0.03	0.02
Rb	0.02	0.02	0.015	0.009	0.007	0.004
Co	0.009	0.008	0.005	0.004	0.002	0.0016
Sb	0.004	0.005	0.004	0.005	0.0044	0.0028
As	0.005	0.0045	0.003	0.003	0.0020	0.0014
Be	0.0008	0.0008	0.0005	0.0003	0.0002	0.0001
Cd	0.0007	0.0007	0.0008	0.0007	0.0006	0.0004
Se	0.0003	0.0003	0.0002	0.0007	0.0008	0.0005
Tl	0.0003	0.0003	0.0002	0.00005	0.00005	0.00003
Metals	46.29 (7)	45.53 (9)	34.29 (12)	20.18 (7)	13.78 (9)	8.38 (6)

In general, OC, EC, metal components, and ions account for 15–37%, 3–10%, 7–12%, and 3–6% of $\text{PM}_{2.5}$, PM_{10} and TSP in Bamako, respectively, whereas these percentages are 22–26%, 7–11%, 6–9%, and 13–25% in Dakar (Table 1). Total carbon (OC + EC) was the most abundant component in the atmospheric particle composition, accounting for 18–47% in Bamako and 32–37% in Dakar. This is consistent with the findings of Val et al. [9], who discovered a high total carbon content at the same sites, using 13-stage impactors. These results are also consistent with the values reported for some European and Asian urban aerosols by Putaud et al. [65], Querol et al. [66], and Yu et al. [67], who estimated contributions of 20–40% and 25–50% to the ambient PM_{10} and $\text{PM}_{2.5}$ mass, respectively. The average EC (OC) concentrations in Bamako for the entire period were 23.3 (102.4) $\mu\text{g}\cdot\text{m}^{-3}$ for TSP, 18.8 (82.4) $\mu\text{g}\cdot\text{m}^{-3}$ for PM_{10} , and 27.1 (102.4) $\mu\text{g}\cdot\text{m}^{-3}$ for $\text{PM}_{2.5}$. In Dakar, the average EC (OC) concentrations were 20.1 (69.2) $\mu\text{g}\cdot\text{m}^{-3}$ for TSP, 16.4 (34.9) $\mu\text{g}\cdot\text{m}^{-3}$ for

PM₁₀, and 15.9 (35.8) $\mu\text{g}\cdot\text{m}^{-3}$ for PM_{2.5}. The results indicate that the EC to OC ratio is higher in Dakar (0.29–0.47) than in Bamako (0.23–0.26). Figure S5 shows that during the dust event in Bamako, carbonaceous particles significantly decrease while elements associated with mineral dust significantly increase in number (especially in TSP and PM₁₀ fractions), highlighting the impact of high dust concentrations on carbonaceous measurements.

The second major compound in Dakar, water-soluble inorganic ions, accounted for 13% of TSP (31.1 $\mu\text{g}\cdot\text{m}^{-3}$), 25% of PM₁₀ (38.9 $\mu\text{g}\cdot\text{m}^{-3}$), and 16% of PM_{2.5} (21.5 $\mu\text{g}\cdot\text{m}^{-3}$). Metal mass concentrations range from 8.4 to 20.2 $\mu\text{g}\cdot\text{m}^{-3}$, representing 6 to 9% of total mass, regardless of size fraction. In Bamako, metal elements were the second most important compounds, accounting for 7% of TSP (46.3 $\mu\text{g}\cdot\text{m}^{-3}$), 9% of PM₁₀ (45.5 $\mu\text{g}\cdot\text{m}^{-3}$), and 12% of PM_{2.5} (34.3 $\mu\text{g}\cdot\text{m}^{-3}$). While water-soluble inorganic ions represented 3–6% of total PM mass (15.7–24.1 $\mu\text{g}\cdot\text{m}^{-3}$). It should be noted that metal elements contribute more to PM_{2.5} than PM₁₀ and TSP, reflecting the impact of fine dust in Bamako's aerosol mass concentration. Aside from the location of the measurement sites in the Sahara and Sahel regions, Bamako and Dakar (to a lesser extent) are characterized by a large number of unpaved roads, which favor particle resuspension from urban sources due to road traffic.

The absolute concentration levels for all components were more important in Bamako than in Dakar, except for the water-soluble compounds, for which concentrations in Dakar were 2–6 times higher than in Bamako. This is related to differences in location and meteorology, since Bamako is located in a basin under strong influence of continental air masses, while Dakar is a typical coastal site with high impact from a sea breeze which facilitates pollutant dispersion.

3.2. Identification and Apportionment of Sources

3.2.1. Enrichment Factor Calculations

In this section, we calculate enrichment factors (EF), which are indicators for interpreting the metal element contributions in each source category. Enrichment factors of atmospheric elements were calculated as the ratio of the concentration of an element X to the concentration of a reference element in an aerosol sample compared to the same ratio in average upper crust geological samples [68], as given in Equation (5):

$$EF = \frac{\left(\frac{X}{E_{ref}}\right)_{aerosol}}{\left(\frac{X}{E_{ref}}\right)_{crust}} \quad (5)$$

where X and E_{ref} , respectively, refer to the concentration (in ppb) of element X and the reference element. Many elements (Al, Ti, Si, Fe, Mn, and Sr), mostly of soil origin, are used as references for E_{ref} [12,68]. EF interpretations widely vary according to authors, due to the uncertainties associated with reference elements.

The results obtained for Bamako and Dakar are reported in Figure 5. EF calculations are performed using Al, Fe and Ti as crustal references [12,68]. Alleman et al. [40] proposed a classification of sources based on EF, which we used in our study. Elements with EF values less than 5 (Al, Co, Cr, Fe, K, Mg, Mn, Na, Rb, Ti, Be, and Tl), regardless of the reference element, are considered of natural origin, whereas elements with EF values greater than 50 (Sb, Cd, and Cu) are generally from anthropogenic activities. As shown in Figure 5, the average EF for Cu, however, exhibits values less than 10 in Bamako and greater than 50 in Dakar, which must be taken into account in the interpretation of sources. Elements with intermediate EF values (between 5 and 50) could originate from both natural and anthropogenic emissions (As, Ca, Ni, V, and Zn). The significant difference in EF for Ni, V, Ca, and Na between Bamako and Dakar indicates that these elements are most likely derived from multiple sources (Figure 5).

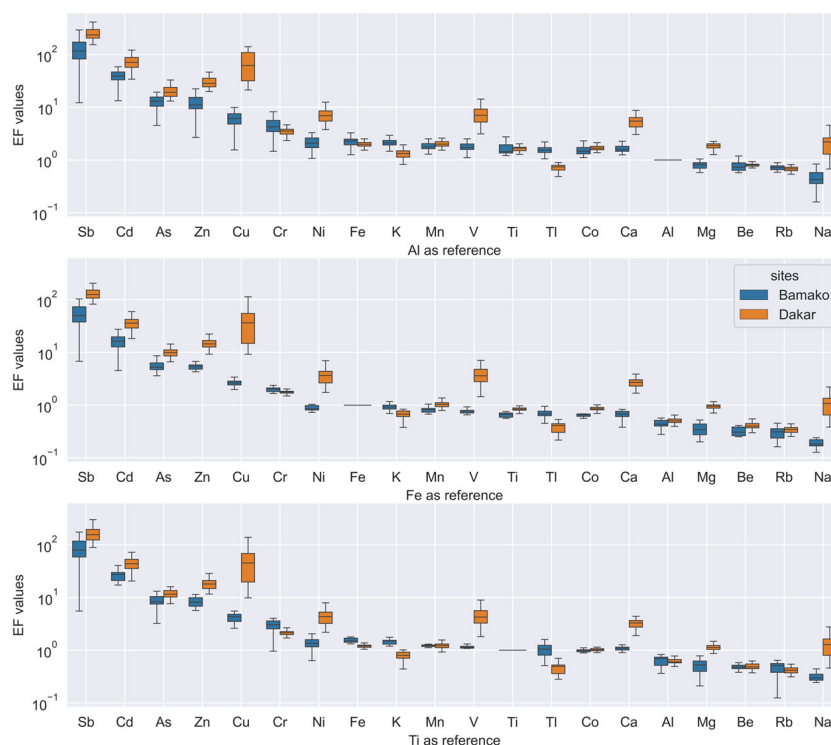


Figure 5. Enrichment factor (EF) values for PM elemental composition calculated in Bamako and Dakar using Al, Fe and Ti as reference elements.

3.2.2. PCA for Source Identification

The factor loadings after rotation for Bamako and Dakar are reported in Table 2. The number of optimal principal components (PCs) for each measurement site is determined based on the eigenvalue, which represents the amount of variance explained by each PC greater than one. The table also displays the variability percentage, which expresses the contribution of each principal component, as well as the cumulative percentage, which represents the progressive accumulation of the variability percentage up to 100%. PCA identified five PCs (PC1 to PC5) or sources in both Bamako and Dakar, accounting for 92.9% and 89.5% of the variance, respectively (Table 2). The factor loadings represent correlations between rotated principal components (PCs) and compounds. Factor loadings greater than 0.600 (highlighted in bold) are considered strong, while those between 0.300 and 0.600 (underlined) are considered moderate [69]. Some compounds have a strong relationship with a specific PC. If these compounds are known to be characteristic of a specific air pollution source, then that source is associated with this PC. Table 3 depicts the possible associations between PCs and pollution sources based on the characteristics of the compounds. However, it is not always possible to clearly link a source to a PC. In this case, prior knowledge of the sampling sites and their possible sources is crucial.

3.2.3. Description of Sources

Finding the physical meaningful and the number of sources (so called factors) is a key step in PMF source apportionment. The PMF was run in various configurations, testing a variety of factors (three to seven factors for each set of samples). To determine the optimal number of factors, the goodness of model fit parameter (Q) was evaluated. The best solution must be related to the F_{peak} range. The rotational freedom of the possible solution is controlled by the F_{peak} parameter. It should be noted that different studies reported that too high positive and negative F_{peak} values result in a poorer fit. As a result, the values investigated here ranged from -1 to 1 in 0.1 step. The optimum solutions for the base run were obtained using five factors or sources in both Bamako and Dakar, corresponding to F_{peak} value of 0.5 , and matching the number of principal components (PCs) obtained

using PCA. The Pearson correlations between the PCs obtained with PCA and the factors derived from the PMF receptor model were calculated to verify the coherence of these source identifications (Table 4). The significant correlations (p values ≤ 0.05) are indicated in bold. The two methods show a strong correspondence, which allows an investigation of the source profiles in Bamako and Dakar. The goal is to identify the nature of the sources by calculating their relative contribution to each of the chemical compounds.

Table 2. Correlations between chemical compounds and principal components (PCs) in Bamako and Dakar (factor loadings ≥ 0.600 are highlighted in bold, while moderate factor loadings (0.300–0.600) are underlined, with categorization based on Nyanganyura et al. [69]).

	Bamako					Dakar				
	PC1	PC2	PC3	PC4	PC5	PC1	PC2	PC3	PC4	PC5
Eigenvalue	15.386	3.180	1.284	1.228	1.012	17.126	3.231	1.560	1.137	1.107
Variability (%)	56.986	11.777	8.459	8.251	7.452	63.431	11.967	5.776	4.210	4.100
Cumulative (%)	56.986	68.763	77.222	85.472	92.924	63.431	75.398	81.174	85.384	89.484
Factor loadings										
Al	0.982	0.051	−0.041	0.035	−0.120	0.688	<u>0.334</u>	<u>0.300</u>	<u>0.341</u>	<u>0.385</u>
As	0.938	0.143	0.206	0.099	−0.111	0.154	<u>0.177</u>	<u>0.470</u>	<u>0.577</u>	0.245
Be	0.976	0.105	−0.086	0.032	−0.143	0.629	<u>0.469</u>	0.237	<u>0.342</u>	<u>0.410</u>
Ca	0.620	<u>0.582</u>	0.167	<u>0.443</u>	0.051	0.294	0.746	0.144	<u>0.399</u>	<u>0.341</u>
Cd	0.184	−0.218	0.251	0.233	0.643	0.277	0.699	0.262	<u>0.441</u>	0.252
Co	0.972	0.143	0.015	0.086	−0.121	<u>0.542</u>	<u>0.347</u>	0.225	<u>0.407</u>	<u>0.596</u>
Cr	0.830	0.291	<u>0.358</u>	0.232	0.074	<u>0.509</u>	0.158	0.259	<u>0.428</u>	0.658
Cu	0.642	0.291	<u>0.512</u>	0.276	0.089	0.097	<u>0.360</u>	<u>0.312</u>	−0.729	−0.107
Fe	0.964	0.181	0.085	0.129	−0.068	0.653	0.293	<u>0.351</u>	<u>0.465</u>	<u>0.362</u>
K	<u>0.370</u>	0.879	0.041	0.236	0.051	0.702	<u>0.415</u>	<u>0.357</u>	0.253	0.282
Mg	0.920	0.241	−0.069	0.181	−0.105	0.620	0.297	<u>0.441</u>	<u>0.453</u>	<u>0.306</u>
Mn	0.974	0.130	0.001	0.079	−0.123	<u>0.594</u>	<u>0.425</u>	<u>0.319</u>	<u>0.481</u>	<u>0.318</u>
Na	0.152	0.930	0.073	0.227	0.071	<u>0.459</u>	0.113	0.782	0.239	0.159
Ni	0.870	0.063	−0.134	0.012	0.119	−0.178	−0.004	−0.049	−0.062	0.949
Rb	0.928	0.059	0.178	0.128	−0.003	0.707	<u>0.394</u>	0.283	<u>0.352</u>	<u>0.306</u>
Sb	−0.202	−0.081	0.892	0.101	<u>0.317</u>	<u>0.546</u>	<u>0.361</u>	<u>0.471</u>	−0.100	0.267
Se	0.841	0.057	0.278	0.299	0.155	0.170	<u>0.363</u>	0.657	−0.319	<u>0.376</u>
Ti	0.977	0.107	−0.056	0.036	−0.134	0.663	<u>0.352</u>	0.282	<u>0.424</u>	<u>0.385</u>
Tl	0.980	0.038	0.095	0.078	−0.013	0.612	<u>0.534</u>	0.184	0.191	<u>0.402</u>
V	0.980	0.124	0.014	0.076	−0.104	<u>0.346</u>	0.636	<u>0.342</u>	−0.161	<u>0.381</u>
Zn	0.264	<u>0.414</u>	0.698	0.294	<u>0.301</u>	<u>0.477</u>	0.659	<u>0.338</u>	0.289	0.173
EC	−0.481	0.201	0.143	0.045	0.753	0.078	<u>0.382</u>	0.073	0.807	0.074
OC	−0.359	<u>0.373</u>	0.288	−0.013	0.742	<u>0.472</u>	0.078	0.117	0.789	0.091
Cl [−]	0.187	<u>0.349</u>	<u>0.443</u>	0.728	0.213	0.197	0.097	0.906	0.152	−0.003
NO ₃ [−]	0.133	<u>0.312</u>	0.095	0.908	0.080	−0.112	<u>0.382</u>	0.832	0.021	0.196
SO ₄ ^{2−}	0.889	0.230	0.004	0.284	−0.058	−0.051	0.778	<u>0.529</u>	−0.042	0.193

Table 3. Principal component (PC) and potential source associations (chemical species with high factor loadings are in bold, while the other species have moderate factor loadings).

	Rotated PCs	Potential Sources	Characteristic Compounds
Bamako	PC1	Dust	Al, As, Be, Cr, Co, Fe, Ti, Mg, Mn, V, Tl, Rb, Se, Ni, SO ₄ ^{2−} , Cu, Ca, K
	PC2	Solid fuel combustion	Na, K, Ca, Zn, NO ₃ [−] , Cl [−] , OC
	PC3	Resuspended road dust	Sb, Zn, Cu, Cl [−] , Cr
	PC4	Secondary aerosols	NO ₃ [−] , Cl [−] , Ca
	PC5	Vehicle	EC, OC, Cd, Zn
Dakar	PC1	Dust	Al, Be, Rb, K, Ti, Tl, Be, Fe, Mg, Co, Mn, Na, Sb, Cr, Zn, OC, V
	PC2	Industries, Oil burning	Ca, Cd, V, Zn, SO ₄ ^{2−} , Tl, K, Mn, Be, NO ₃ [−] , EC, Ti, Al, Sb, Se, Rb, Cu
	PC3	Salts	Na, Cl [−] , NO ₃ [−] , Se, SO ₄ ^{2−} , As, K, Mg, Al, Cu, Fe, Mn, Sb, V
	PC4	Vehicle	EC, OC, Cd, Co, Cr, Fe, Mg, Mn, As, Al, Be, Ti, Ca, Rb
	PC5	Resuspend road particles	Ni, Cr, Co, Be, Al, Tl, Ca, Fe, Mg, Mn, Rb, Se, Ti, V

Table 4. Pearson correlations between PCA principal components (PCs) and PMF model sources (Factors). The significant positive correlations are highlighted in bold. p values ≤ 0.05 were used to determine significance.

Bamako	Factor 1	Factor 2	Factor 3	Factor 4	Factor 5
PC1	−0.72	0.00	−0.07	0.84	−0.06
PC2	−0.13	−0.46	0.82	−0.40	0.10
PC3	0.30	0.71	−0.13	−0.63	−0.07
PC4	−0.22	0.19	−0.01	−0.56	0.78
PC5	0.81	0.13	−0.17	−0.70	−0.05
Dakar	Factor 1	Factor 2	Factor 3	Factor 4	Factor 5
PC1	−0.24	0.14	−0.33	0.84	−0.34
PC2	−0.32	−0.13	−0.18	0.28	0.57
PC3	0.89	−0.38	−0.34	−0.33	0.05
PC4	−0.16	0.78	−0.15	0.28	−0.72
PC5	−0.35	−0.11	0.57	0.32	−0.38

Bamako

From PMF output, the comparison of reconstructed daily mean PM concentrations from all sources with measured PM concentrations demonstrates that the identified factors effectively reproduce measured masses. Table S8 (Supplementary Materials) compares calculated values with measured concentrations for each species to assess the performance of the PMF model. The largest uncertainties, such as 15% for Ni, 16% for EC and 14% for OC, and the low correlation coefficients can be attributed to data quality because EC and OC missing values were replaced by their median values and associated uncertainties were assigned as four times the mean values. However, in general, significant correlation coefficients were obtained between measured and calculated concentrations.

Motor vehicles: High factor loadings (0.742–0.753) were obtained for this factor in PCA (Table 2, PC5) and high contributions (83–94%) in PMF (Figure 6), both for OC and EC, which can be linked with fuel combustion emissions [70]. Several authors [71–73] have reported OC/EC mass concentration ratios of 1.1 for traffic emissions, 3.3 for secondary organic carbon formation, 6.6 for biofuel combustion and 12 for long-range transport. The OC/EC ratio for this factor ranges from 3.8 to 4.4 in Table 2, indicating probable mixtures of various combustion sources such as two-wheel two-stroke vehicles (using a mixture of oil and gasoline), personal and public cars also using poor quality gasoline. The high Cd (0.643) and moderate Sb (0.317) and Zn (0.301) loadings, as well as their presence in PMF (26%, 39% and 18%, respectively), support tire wear and brakes lining residuals [74,75] as a contributing source.

Resuspended road dust: In PMF, Sb (61%), Zn (51%) and Cd (48%) dominate in this factor. Cr and Cu (45% and 44%, respectively) also contribute to this source, as well as mineral dust tracers such as As (38%), Fe (30%) and Ca (24%) (Figure 6). In the PCA results, Sb and Zn have also the highest factor loadings (0.892 and 0.698, respectively), while Cr and Cu have moderate loadings (Table 2, PC3). Sb, Zn and Cd trends in Bamako did not show peaks during the dust episode (Figure S5), indicating that these elements are primarily emitted by anthropogenic activities such as brakes and tire wear [74,75], fuel combustion, or biomass burning [76,77]. All of these point sources were present near the site, with open waste burning occurring in Bamako in the evenings. Furthermore, the high EF values reported in Figure 5 support the anthropogenic origin of these elements [40]. According to some studies [76,77], particles from both natural and anthropogenic sources may aggregate in the soil before being resuspended as a result of vehicle traffic. This explains why this source could be classified as traffic. The majority of unpaved roads surrounding the measurement site favor the presence of dust in the factor.

Solid fuel combustion: This factor was notable for its high Na and K contributions to total PM mass, which were around 99% for Na and 75% for K in the PMF analysis (Figure 6). Furthermore, in the PCA, these two species have the highest factor loadings (0.879–0.930)

(Table 2, PC2). K is a tracer typical for emissions from wood combustion [46]. Zn, Fe, Cr and Co are also abundant in this factor, accounting for about 20% of the total mass of each species, reflecting the importance of emissions from common local activities at the sampling site, such as residential combustions for cooking, street food preparation, traditional forges, smelters, open waste burning and unidentified combustion sources. Cr emissions from coal combustion for power generation and waste incineration are well established [16]. Because of the mix of anthropogenic combustion sources, we can conclude that this factor is most likely related to solid fuel combustions.



Figure 6. Profiles of the five factors identified by the PMF in Bamako.

Crustal dust: This factor is characterized by high contributions of Ti (67%), Be (70%), Mn (58%), Co (56%), V (56%), Al (63%), and Fe (46%) (Figure 6), with the majority of them exhibiting high loadings in the PCA results (Table 2, PC1). Metals were the second most abundant component in Bamako. Al was the most abundant metal found in all particle modes (Table 1), with average daily concentrations of 17.9 $\mu\text{g.m}^{-3}$ in $\text{PM}_{2.5}$, 22.2 $\mu\text{g.m}^{-3}$ in PM_{10} , and 21.2 $\mu\text{g.m}^{-3}$ in TSP, followed by Fe, which had values of 14.3 $\mu\text{g.m}^{-3}$ in $\text{PM}_{2.5}$, 20.4 $\mu\text{g.m}^{-3}$ in PM_{10} , and 21.9 $\mu\text{g.m}^{-3}$ in TSP. During the dust episode, daily Al and Fe concentrations rose by nearly a factor of 13 (from 6.3 to 82.2 $\mu\text{g.m}^{-3}$) and 12 (from 5.3 to 66.7 $\mu\text{g.m}^{-3}$), respectively. The peak concentrations of Al and Fe during the dust episode (Figure S5) are very close to the values reported by Adepetu et al. [78] in typical continental crustal rocks of 81.3 and 50 $\mu\text{g.m}^{-3}$, respectively. The average Fe/Al ratio varies from 0.79 ($\text{PM}_{2.5}$) to 1.03 (TSP). These values are comparable to those reported in the literature for typical crustal dust elements [46,79], which is consistent with their enrichment factors (EF) close to unity, regardless of the reference element (Figure 5). This source is most likely due to Saharan desert crustal dust predominating in PM concentrations during dust storms.

Secondary aerosols: This factor contains significant contributions from NO_3^- (65%), Cl^- and Mg (53%), SO_4^{2-} (45%), and Ca (43%) (Figure 6). The PCA results also show that some of these compounds have high factor loadings (0.908 for NO_3^- and 0.728 for Cl^-) and Ca has moderate loading (0.443) (Table 2, PC4). Except for Mg and Ca, none of these water-soluble species showed a peak during the dust episode (Figure S5), indicating sources other than dust. SO_4^{2-} in this factor could result from heterogeneous processes in the presence of dust. Because the concentrations of non-soluble Mg and Ca peak during the dust episode, a fraction of these two compounds can be considered from crustal dust. This is consistent with the EF values of less than 1 for these two elements (Figure 5). Ca is also a common tracer typical of emissions from building construction and cement production [80]. NO_3^- and Cl^- are also linked to anthropogenic activities [46,81]. Chemical processes in dust wells present during the field campaign may result in secondary aerosol formation because Bamako is located in a basin with low wind speeds and high temperatures that favor gas-to-particle conversion mechanisms [82]. This source results from the interaction of compounds primarily from anthropogenic (NO_3^- , Cl^-) and natural (Mg, Ca) sources.

Dakar

The identified factors effectively reproduce measured masses when daily mean reconstructed PM concentrations from all sources are compared to measured values. Table S9 (Supplementary Materials) compares the measured and calculated concentrations for each species in Dakar. Uncertainties are generally low, with the highest being 10% for PM as a result of including PM as a variable and assigning an uncertainty value four times the PM concentration values [83,84]. Significant correlation coefficients are also obtained between modeled and measured specie concentrations.

Sea salts: This source is characterized by high contributions of Cl^- (97%) and Na (80%), and the moderate presence of Mg (29%) (Figure 7). PCA analysis also reveals that these elements have high factor loadings (0.906, 0.782, and 0.441, respectively) (Table 2, PC3). These three species account for 40, 24 and 3% of the total mass of this aerosol source, respectively, in close agreement with their corresponding percentages in seawater, which are 55, 30 and 3%, respectively [85]. The ratios Na/Mg and K/Mg were investigated to confirm the marine origin of these elements. The calculated ratio of 8.3 is very close to the 8.4 found in sea water [86]. Yuan et al. [87] and Alleman et al. [40] also found values of 8.4 and 8.5, respectively. The calculated K/Mg ratio for this factor (0.34) is also of the same order as in sea water (0.31) [86]. This source also contains NO_3^- (53%) and SO_4^{2-} (31%) species with loadings in the PCA of 0.832 and 0.529, respectively. As a result of condensation processes, sulfate and nitrate may be found in marine aerosols [80]. This is consistent with Dakar being surrounded on three sides by the Atlantic Ocean (Figure 1).

Motor Vehicles: This source contains 86% of the total OC, 62% of the total EC, 68% of the total As (Figure 7), and PCA results show the highest factor loadings of 0.807, 0.789 and 0.577 for these species, respectively (Table 2, PC4). These species are common combustion tracers, such as motor vehicle exhaust fumes [80,88]. The OC/EC ratio of 3.3 is comparable to the value found in Pio et al. [73] for traffic diesel and gasoline emissions. This value is of the same order as previously reported, namely 2.1 ± 1.0 obtained from 13-stage impactors in Dakar [9]. PCA results also show that this factor contributes to the observed concentrations of Cd, Ca, Fe, Ti, Co, Cr, Mn, Sb, Rb, and Mg, with moderate factor loadings (0.340–0.480). The corresponding contributions from PMF analysis ranged from 20 to 44%. Some of these elements are typically produced by natural sources (Ti, Fe, Cr, Co, and Mn), anthropogenic activities (Cd, Sb) or both sources (As, Ca). This implies the possibility of natural compounds aggregating with fresh aerosols from motor vehicles.

Industries and oil burning: This source is characterized by high Ni (100%) and Zn (66%) contributions, as well as moderate Cr and Co contributions (Figure 7). PCA analysis also reveals high factor loadings for Ni (0.949), Cr (0.658) and moderate loadings for Co (0.596) and Se (0.376) (Table 2, PC5). The presence of these elements in this factor indicated oil combustion emissions [80,89] related to hydrocarbon storage and transit at

the industrial area of Dakar's port, which is close to the measurement site (less than 1 km) (Figure 1). Zn is also produced by lubricating oil combustion and tire wear [76]. Additional species (Cr, Co, and Se) in this factor are most likely related to industrial activities such as manufacturing, local smelters, and activities like car repair. The measurement site was close to the two biggest car parks in Dakar and the industrial area located in the northeast of the measurement site. In addition, winds from northeast prevailed throughout the campaign on average (Figure 1).

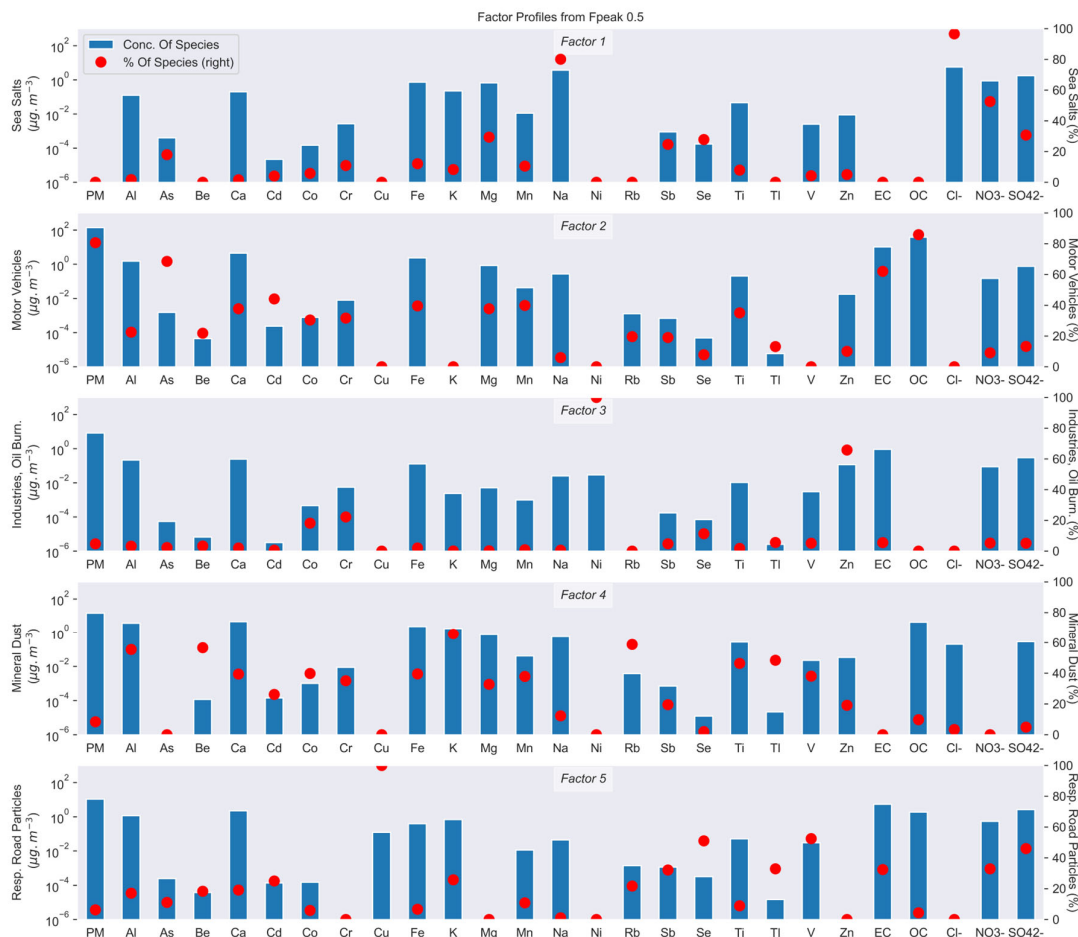


Figure 7. Profiles of the five factors identified by the PMF in Dakar.

Mineral dust: This factor reveals high loadings of Al, Be, Ti, and Fe in PCA, generally greater than 0.6 (Table 2, PC1), and contains high contributions of these elements ranging from 40% to 60% in PMF (Figure 7). Additional elements such as Rb, Co, Cr and Mn are also abundant in this factor. EF calculations (Figure 5) show that all of these elements have values close to unity, confirming their natural origin [12,16,80,90]. This result is consistent with mineral dust.

Resuspended road particles: This factor has high contributions of Cu (100%), V (52%), Se (51%), SO_4^{2-} (46%), and moderate contributions of Cd, K, Sb, Tl, EC, and NO_3^- (25–30%) (Figure 7). PCA also exhibits significant loadings of V, SO_4^{2-} , Cd, Zn (>0.600), and moderate loadings of Se, K, Sb, Tl, EC, and NO_3^- (0.300–0.600) (Table 2, PC2). Cu, Sb, and Cd are thought to be anthropogenic due to their high EF values (>50) (Figure 5). Cu and Sb are components of brake linings [74,75], while Se, K are good tracers for coal/wood combustion [91,92]. SO_4^{2-} in this factor could result from heterogeneous processes in the presence of dust. The presence of all these compounds indicates that this factor comes from a variety of sources. These compounds were resuspended by road traffic after being aggregated through complex processes.

3.2.4. Source Apportionment via PMF

Only PM₁₀ and PM_{2.5} source contributions based on PCA/PMF in Bamako and Dakar are displayed due to their importance in health studies (Figure 8). Traffic emissions include motor vehicles (vehicular and two-wheel two-stroke) and resuspended road dust. At Bamako, this source comprised 47% of PM_{2.5} and 45% of PM₁₀ masses, due to the fact that a large proportion of Bamako's population driving two-wheel two-stroke vehicles, the frequent traffic congestion throughout the city, and the street qualities, which are mostly cobble or unpaved. Only a few major streets use asphalt. Crustal dust was the second dominant source of PM₁₀ mass (30%), but remains an important source of PM_{2.5} fraction (24%). This can be explained by the measurement period in the dry season, when the Harmattan winds brought dust from the Sahara Desert. Two additional sources were identified: one defined as secondary aerosols, which contributed 16% and 10% of the PM₁₀ and PM_{2.5} masses, respectively, and another identified as solid fuel combustion, which accounted for 13% of the total PM₁₀ and 16% of the total PM_{2.5} (Figure 8a).

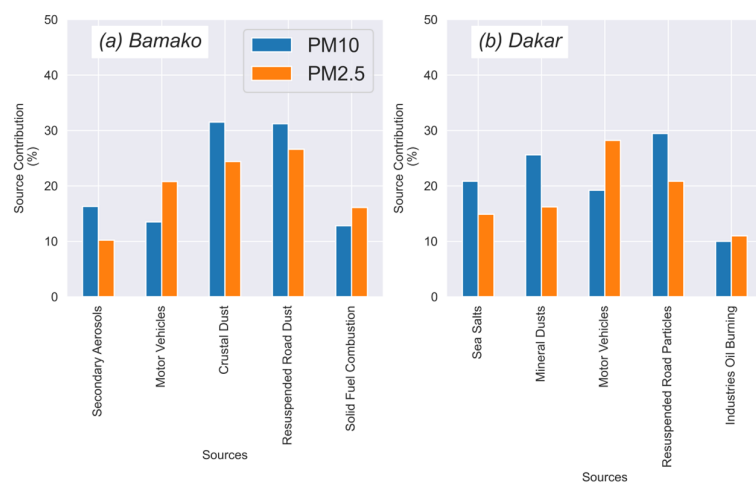


Figure 8. PM₁₀ and PM_{2.5} source contributions estimated by PMF in (a) Bamako and (b) Dakar.

Traffic emissions, as expected, are the most significant source of PM₁₀ and PM_{2.5} at the Dakar site, accounting for approximately 49% of total PM₁₀ and PM_{2.5} concentrations (Figure 8b). It should be noted that majority of Senegal's vehicle fleet (more than half) operate in Dakar and are predominately powered by outdated diesel engines. Old diesel vehicles account for more than 60% of Dakar's public transportation. The proportion of marine aerosols or sea salts in PM₁₀ (20%) is slightly higher than in PM_{2.5} (15%). Mineral dust, which contributes approximately 25% and 16% of the aerosol mass on average for PM₁₀ and PM_{2.5} mass concentrations, was the second most important source, as it was in Bamako. The industrial sector and oil-burning activities together contributed about 10–11% of the measured PM₁₀ and PM_{2.5} concentrations (Figure 8b). The identification of this source can be explained by the location of the port industrial zone close to the sampling site (Figure 1), where oil refinery activities and the storage and transit of hydrocarbons were carried out. Using a year of measurements (2018–2019), Kebe et al. [64] identified the same four sources in Dakar: traffic emissions, mineral dust, industrial emissions and sea salt/secondary aerosols. However, they did not quantify their contribution to PM_{2.5} mass for a comparison with our study.

According to our findings in both Bamako and Dakar cities, anthropogenic activities are the primary sources of air pollution in West Africa, accounting for 60–65% of the total concentration, regardless of PM mode.

4. Conclusions

To identify the levels and the major sources of air pollution, this paper characterizes the concentrations of PM (TSP, PM₁₀ and PM_{2.5}) and their chemical composition at two West

African traffic sites (Bamako in Mali and Dakar in Senegal). Carbonaceous aerosols (OC, EC), major ions (Na^+ , K^+ , Mg^{2+} , Ca^{2+} , SO_4^{2-} , NO_3^- , and Cl^-) and 21 metal elements were analyzed. Daily $\text{PM}_{2.5}$ and PM_{10} concentrations in the dry season exceeded the WHO's 24 h air quality guidelines established in 2005 of 25 and $50 \mu\text{g}\cdot\text{m}^{-3}$, respectively.

Using PCA and PMF methodologies, five sources were extracted and quantified in both Bamako (crustal dust, resuspended road dust, solid fuel combustion, motor vehicles and secondary aerosols) and Dakar (resuspended road particles, mineral dust, sea salts, motor vehicle emissions, and industries and oil combustion). The traffic sector, which includes motor vehicle emissions and resuspended road dust, was the dominant source of compounds in $\text{PM}_{2.5}$ and PM_{10} at both sites (45–49%). As a result, anthropogenic sources predominated, contributing up to 60–65% of the PM mass. These measurements were taken in 2009, and this detailed analysis could serve as a basis for future research on how the composition of particulate matter in African capitals has changed since the late 2000s.

Supplementary Materials: The following supporting information can be downloaded at: <https://www.mdpi.com/article/10.3390/atmos14040684/s1>, Figure S1: Daily evolution of $\sigma_{\text{abs}}/\sigma_{\text{scat}}$ ratio in Bamako and Dakar; Figure S2: Comparison between average concentration of field blanks and filter blanks; Figure S3: Comparison of calcium, sodium, potassium and magnesium elements measured by ICP-MS and IC, excluded the dust episode; Figure S4: Comparison between the Thermal-Optical Reflectance (TOR) and the THERMAL (THE) methods at the two sites for TC, OC and EC. The linear regression results are displayed, S being the slope for Dakar (S_{Dakar}) and Bamako (S_{Bamako}) with zero intercept; Figure S5: Time variations of $\text{PM}_{2.5}$, PM_{10} and TSP components concentrations measured at Bamako between 20 January and 1 February 2009; Figure S6: Time variations of components in $\text{PM}_{2.5}$, PM_{10} and TSP concentrations measured at Dakar between 1 and 13 December 2009; Table S1: Detection limits and blank values for water soluble species. The analysis was performed on 24 filter blanks and all values are in ppb; Table S2: Detection limits, vessel blank (VB) and filter blank (FB) in a matrix of 10 ml HNO_3 and 0.5 ml HF; Table S3: Certified/non certified and resulting concentration for elements in SRM 1648; Table S4: Summary of the Thermal Optical Reflectance (TOR) and THERMAL (THE) protocols; Table S5: Comparison of no decarbonation (noDC) and decarbonation (DC) procedures on OC, EC and TC (OC + EC) measurements at Bamako; Table S6: Comparison of no decarbonation (noDC) and decarbonation (DC) procedures on OC, EC and TC (OC + EC) measurements at Dakar; Table S7: Quality control performance measures for carbonaceous analyses in Bamako and Dakar; Table S8: Comparison between measured and PMF calculated concentrations (in $\text{ng}\cdot\text{m}^{-3}$) except for PM (in $\mu\text{g}\cdot\text{m}^{-3}$) in Bamako for studied chemical species; Table S9: Comparison between measured and PMF calculated concentrations (in $\text{ng}\cdot\text{m}^{-3}$) except for PM (in $\mu\text{g}\cdot\text{m}^{-3}$) in Dakar for all chemical species.

Author Contributions: Conceptualization, T.D. and C.L.; methodology, T.D., C.L. and C.G.-L.; validation, T.D., E.G. and C.L.; formal analysis, T.D., M.-R.O.-L., E.G. and C.Z.; investigation, T.D., C.L., C.G.-L., S.A.N., V.Y. and M.-R.O.-L.; writing—original draft preparation, T.D., C.L. and C.G.-L.; writing—review and editing, T.D., C.L. and C.G.; visualization, T.D.; supervision, C.L. All authors have read and agreed to the published version of the manuscript.

Funding: This research was funded by the CORUS 2 program (Cooperation for Academic and Scientific Research), grant number 94-2009 and has been supported in part by the AQ-WATCH (Air Quality: Worldwide Analysis and Forecasting of Atmospheric Composition for Health) project funded by the European Commission under grant 870301.

Institutional Review Board Statement: Not applicable.

Informed Consent Statement: Not applicable.

Data Availability Statement: The data presented in this study are available on request from the corresponding author.

Acknowledgments: The authors would like to thank the CORUS2 POLCA and AMMA2 programs. We also want to thank the Paul Sabatier University for their financial support, the University of Bamako and the Laboratory of Atmospheric Physics and Oceanographic—Simeon Fongang at the University Cheikh Anta Diop of Dakar for their collaboration. Cyril Zouiten and the GET laboratory (Géosciences Environnement Toulouse) are acknowledged for element trace analysis.

Conflicts of Interest: The authors declare no conflict of interest.

References

1. Pachauri, R.K.; Reisinger, A. *AR4 Climate Change 2007: Synthesis Report. Contribution of Working Groups I, II and III to the Fourth Assessment Report of the Intergovernmental Panel on Climate Change*; Core Writing Team, Pachauri, R.K., Reisinger, A., Eds.; IPCC: Geneva, Switzerland, 2007; Available online: <https://www.ipcc.ch/report/ar4/syr/> (accessed on 28 March 2023).
2. Dockery, D.W.; Pope, C.A. Acute Respiratory Effects of Particulate Air Pollution. *Annu. Rev. Public Health* **1994**, *15*, 107–132. [[CrossRef](#)] [[PubMed](#)]
3. Pope III, C.A.; Burnett, R.T.; Thun, M.J.; Calle, E.E.; Krewski, D.; Ito, K.; Thurston, G.D. Lung cancer, cardiopulmonary mortality, and long-term exposure to fine particulate air pollution. *JAMA J. Am. Med. Assoc.* **2002**, *287*, 1132–1141. Available online: <http://www.ncbi.nlm.nih.gov/pubmed/11879110> (accessed on 10 September 2012).
4. Hamanaka, R.B.; Mutlu, G.M. Particulate Matter Air Pollution: Effects on the Cardiovascular System. *Front. Endocrinol.* **2018**, *9*, 680. [[CrossRef](#)] [[PubMed](#)]
5. Huang, S.-L.; Hsu, M.-K.; Chan, C.-C. Effects of submicrometer particle compositions on cytokine production and lipid peroxidation of human bronchial epithelial cells. *Environ. Health Perspect.* **2003**, *111*, 478–482. Available online: <https://www.ncbi.nlm.nih.gov/pmc/articles/PMC1241431/> (accessed on 28 March 2023).
6. Seagrave, J.; McDonald, J.D.; Bedrick, E.; Edgerton, E.S.; Gigliotti, A.P.; Jansen, J.J.; Ke, L.; Naeher, L.P.; Seilkop, S.K.; Zheng, M.; et al. Lung Toxicity of Ambient Particulate Matter from Southeastern, U.S. Sites with Different Contributing Sources: Relationships between Composition and Effects. *Environ. Health Perspect.* **2006**, *114*, 1387–1393. [[CrossRef](#)] [[PubMed](#)]
7. Lelieveld, J.; Evans, J.S.; Fnais, M.; Giannadaki, D.; Pozzer, A. The contribution of outdoor air pollution sources to premature mortality on a global scale. *Nature* **2015**, *525*, 367–371. [[CrossRef](#)] [[PubMed](#)]
8. Happonen, M.S.; Hirvonen, M.-R.; Hälinen, A.I.; Jalava, P.I.; Pennanen, A.; Sillanpää, M.; Hillamo, R.; Salonen, R.O. Chemical Compositions Responsible for Inflammation and Tissue Damage in the Mouse Lung by Coarse and Fine Particulate Samples from Contrasting Air Pollution in Europe. *Inhal. Toxicol.* **2008**, *20*, 1215–1231. [[CrossRef](#)]
9. Val, S.; Lioussse, C.; Doumbia, E.H.T.; Galy-Lacaux, C.; Cachier, H.; Marchand, N.; Badel, A.; Gardrat, E.; Sylvestre, A.; Baeza-Squiban, A. Physico-chemical characterization of African urban aerosols (Bamako in Mali and Dakar in Senegal) and their toxic effects in human bronchial epithelial cells: Description of a worrying situation. *Part. Fibre Toxicol.* **2013**, *10*, 10–16. [[CrossRef](#)]
10. Bertrand, J.; Baudet, J.; Drochon, A. Importance des Aérosols Naturels en Afrique de l’Ouest. *J. Rech. Atmos.* **1974**, 845–860. Available online: http://bibliotheque.meteo.fr/exl-php/cadcgp.php?CMD=CHERCHE&MODELE=vues/mf_-_internet_recherche_avancee_anonyme/tpl-r.html&WHERE_IS_DOC_REF_LIT=QUE00025379&&TABLE=ILS_DOC (accessed on 13 February 2023).
11. Asubiojo, O.I.; Obioh, I.B.; Oluyemi, E.A.; Oluwole, A.F.; Spyrou, N.M.; Farooqi, A.S.; Arshed, W.; Akanle, O.A. Elemental characterization of airborne particulates at two Nigerian locations during the Harmattan season. *J. Radioanal. Nucl. Chem.* **1993**, *167*, 283–293. [[CrossRef](#)]
12. Eltayeb, M.A.H.; Injuk, J.; Maenhaut, W.; Van Grieken, R.E. Elemental Composition of Mineral Aerosol Generated from Sudan Sahara Sand. *J. Atmos. Chem.* **2001**, *40*, 247–273. [[CrossRef](#)]
13. Deboudt, K.; Flament, P.; Choël, M.; Gloter, A.; Sobanska, S.; Colliex, C. Mixing state of aerosols and direct observation of carbonaceous and marine coatings on African dust by individual particle analysis: Mixing State and Coating in African Dust. *J. Geophys. Res. Atmos.* **2010**, *115*, D24. [[CrossRef](#)]
14. Arku, R.E.; Vallarino, J.; Dionisio, K.L.; Willis, R.; Choi, H.; Wilson, J.G.; Hemphill, C.; Agyei-Mensah, S.; Spengler, J.D.; Ezzati, M. Characterizing air pollution in two low-income neighborhoods in Accra, Ghana. *Sci. Total Environ.* **2008**, *402*, 217–231. [[CrossRef](#)] [[PubMed](#)]
15. Kouassi, K.S.; Billet, S.; Garāşon, G.; Verdin, A.; Diouf, A.; Cazier, F.; Djaman, J.; Courcot, D.; Shirali, P. Oxidative damage induced in A549 cells by physically and chemically characterized air particulate matter (PM_{2.5}) collected in Abidjan, Côte d’Ivoire. *J. Appl. Toxicol.* **2009**, *30*, 310–320. [[CrossRef](#)]
16. Weinstein, J.P.; Hedges, S.R.; Kimbrough, S. Characterization and aerosol mass balance of PM_{2.5} and PM₁₀ collected in Conakry, Guinea during the 2004 Harmattan period. *Chemosphere* **2010**, *78*, 980–988. [[CrossRef](#)]
17. Dionisio, K.; Rooney, M.S.; Arku, R.E.; Friedman, A.B.; Hughes, A.F.; Vallarino, J.; Agyei-Mensah, S.; Spengler, J.D.; Ezzati, M. Within-Neighborhood Patterns and Sources of Particle Pollution: Mobile Monitoring and Geographic Information System Analysis in Four Communities in Accra, Ghana. *Environ. Health Perspect.* **2010**, *118*, 607–613. [[CrossRef](#)] [[PubMed](#)]
18. Assamoi, E.-M.; Lioussse, C. A new inventory for two-wheel vehicle emissions in West Africa for 2002. *Atmos. Environ.* **2010**, *44*, 3985–3996. [[CrossRef](#)]
19. Doumbia, E.H.T.; Lioussse, C.; Galy-Lacaux, C.; Ndiaye, S.A.; Diop, B.; Ouafou, M.; Assamoi, E.M.; Gardrat, E.; Castera, P.; Rosset, R.; et al. Real time black carbon measurements in West and Central Africa urban sites. *Atmos. Environ.* **2012**, *54*, 529–537. [[CrossRef](#)]
20. Mukherjee, A.; Agrawal, M. World air particulate matter: Sources, distribution and health effects. *Environ. Chem. Lett.* **2017**, *15*, 283–309. [[CrossRef](#)]
21. Gnamien, S.; Yoboué, V.; Lioussse, C.; Ossouhou, M.; Keita, S.; Bahino, J.; Siélé, S.; Diaby, L. Particulate Pollution in Korhogo and Abidjan (Cote d’Ivoire) during the Dry Season. *Aerosol Air Qual. Res.* **2021**, *21*, 200201. [[CrossRef](#)]

22. Larsen, R.K.; Baker, J.E. Source Apportionment of Polycyclic Aromatic Hydrocarbons in the Urban Atmosphere: A Comparison of Three Methods. *Environ. Sci. Technol.* **2003**, *37*, 1873–1881. [CrossRef]
23. Yang, H.; Yu, J.Z.; Ho, S.S.H.; Xu, J.; Wu, W.-S.; Wan, C.H.; Wang, X.; Wang, L. The chemical composition of inorganic and carbonaceous materials in PM_{2.5} in Nanjing, China. *Atmos. Environ.* **2005**, *39*, 3735–3749. [CrossRef]
24. Xu, L.; Chen, X.; Chen, J.; Zhang, F.; He, C.; Du, K.; Wang, Y. Characterization of PM₁₀ atmospheric aerosol at urban and urban background sites in Fuzhou city, China. *Environ. Sci. Pollut. Res.* **2012**, *19*, 1443–1453. [CrossRef] [PubMed]
25. Gordon, G.E. Receptor models. *Environ. Sci. Technol.* **1988**, *22*, 1132–1142. [CrossRef] [PubMed]
26. Hopke, P.K. An introduction to receptor modeling. *Chemom. Intell. Lab. Syst.* **1991**, *10*, 21–43. [CrossRef]
27. Henry, R.C. History and fundamentals of multivariate air quality receptor models. *Chemom. Intell. Lab. Syst.* **1997**, *37*, 37–42. Available online: <http://cat.inist.fr/?aModele=afficheN&cpsidt=10777286> (accessed on 25 September 2012). [CrossRef]
28. Watson, J.G.; Zhu, T.; Chow, J.C.; Engelbrecht, J.; Fujita, E.M.; Wilson, W.E. Receptor modeling application framework for particle source apportionment. *Chemosphere* **2002**, *49*, 1093–1136. [CrossRef] [PubMed]
29. Paatero, P.; Tapper, U. Analysis of different modes of factor analysis as least squares fit problems. *Chemom. Intell. Lab. Syst.* **1993**, *18*, 183–194. [CrossRef]
30. Song, Y.; Xie, S.; Zhang, Y.; Zeng, L.; Salmon, L.G.; Zheng, M. Source apportionment of PM_{2.5} in Beijing using principal component analysis/absolute principal component scores and UNMIX. *Sci. Total Environ.* **2006**, *372*, 278–286. [CrossRef]
31. Callén, M.; de la Cruz, M.; López, J.; Navarro, M.; Mastral, A. Comparison of receptor models for source apportionment of the PM₁₀ in Zaragoza (Spain). *Chemosphere* **2009**, *76*, 1120–1129. [CrossRef]
32. Zhang, R.; Han, Z.; Shen, Z.; Cao, J. Continuous measurement of number concentrations and elemental composition of aerosol particles for a dust storm event in Beijing. *Adv. Atmos. Sci.* **2008**, *25*, 89–95. [CrossRef]
33. Adon, M.; Yoboué, V.; Galy-Lacaux, C.; Lioussé, C.; Diop, B.; Doumbia, E.H.T.; Gardrat, E.; Ndiaye, S.A.; Jarnot, C. Measurements of NO₂, SO₂, NH₃, HNO₃ and O₃ in West African urban environments. *Atmos. Environ.* **2016**, *135*, 31–40. [CrossRef]
34. DNSI. Mali—Recensement Général de la Population et de L’habitat (2009); Direction Nationale de la Statistique et de L’informatique, (DNSI)—Ministère de L’économie et du Plan, Mali, MLI-INSTAT-RGPH-2009. 2019. Available online: <https://demostaf.web.ined.fr/index.php/catalog/348> (accessed on 24 March 2023).
35. ANSD. *Rapport National sur la Situation économique et Sociale du Sénégal, Démographie*, 2009th ed.; Agence National de la Statistique et de la Démographie: Dakar, Senegal, 2009; Available online: https://www.ansd.sn/ressources/ses/chapitres/1-Demographie_2009.pdf (accessed on 1 March 2023).
36. Ouafu-Leumbe, M.-R.; Galy-Lacaux, C.; Lioussé, C.; Pont, V.; Akpo, A.; Doumbia, T.; Gardrat, E.; Zouiten, C.; Sigha-Nkamdjou, L.; Ekodeck, G.E. Chemical composition and sources of atmospheric aerosols at Djougou (Benin). *Meteorol. Atmos. Phys.* **2017**, *130*, 591–609. [CrossRef]
37. Lyamani, H.; Olmo, F.J.; Alados-Arboledas, L.; Reyes, F.J.O. Light scattering and absorption properties of aerosol particles in the urban environment of Granada, Spain. *Atmos. Environ.* **2008**, *42*, 2630–2642. [CrossRef]
38. Esteve, A.; Estelles, V.; Utrillas, M.P.; Martínez-Lozano, J.A. In-situ integrating nephelometer measurements of the scattering properties of atmospheric aerosols at an urban coastal site in western Mediterranean. *Atmos. Environ.* **2012**, *47*, 43–50. [CrossRef]
39. Adon, M.; Galy-Lacaux, C.; Yoboué, V.; Delon, C.; Lacaux, J.P.; Castera, P.; Gardrat, E.; Pienaar, J.; Al Ourabi, H.; Laouali, D.; et al. Long term measurements of sulfur dioxide, nitrogen dioxide, ammonia, nitric acid and ozone in Africa using passive samplers. *Atmos. Meas. Tech.* **2010**, *10*, 7467–7487. [CrossRef]
40. Alleman, L.Y.; Lamaison, L.; Perdrix, E.; Robache, A.; Galloo, J.-C. PM₁₀ metal concentrations and source identification using positive matrix factorization and wind sectoring in a French industrial zone. *Atmos. Res.* **2010**, *96*, 612–625. [CrossRef]
41. Pakkanen, T.A.; Kerminen, V.-M.; Korhonen, C.H.; Hillamo, R.E.; Aarnio, P.; Koskentalo, T.; Maenhaut, W. Urban and rural ultrafine (PM_{0.1}) particles in the Helsinki area. *Atmos. Environ.* **2001**, *35*, 4593–4607. [CrossRef]
42. Celso, V.; Dabek-Zlotorzynska, E.; Mathieu, D.; Okonskaia, I. Validation of a Simple Microwave-Assisted Acid Digestion Method Using Microvessels for Analysis of Trace Elements in Atmospheric PM_{2.5} in Monitoring and Fingerprinting Studies. *Open Chem. Biomed. Methods J.* **2010**, *3*, 143–152. Available online: <https://benthamopen.com/ABSTRACT/TOCBMJ-3-143> (accessed on 28 March 2023).
43. Swami, K.; Judd, C.D.; Orsini, J.; Yang, K.X.; Husain, L. Microwave assisted digestion of atmospheric aerosol samples followed by inductively coupled plasma mass spectrometry determination of trace elements. *Fresenius J. Anal. Chem.* **2001**, *369*, 63–70. [CrossRef] [PubMed]
44. Sandroni, V.; Smith, C.M. Microwave digestion of sludge, soil and sediment samples for metal analysis by inductively coupled plasma–atomic emission spectrometry. *Anal. Chim. Acta* **2002**, *468*, 335–344. [CrossRef]
45. Andreae, M.; Browell, E.V.; Garstang, M.; Gregory, G.L.; Harriss, R.C.; Hill, G.F.; Jacob, D.J.; Pereira, M.C.; Sachse, G.W.; Setzer, A.W.; et al. Biomass-burning emissions and associated haze layers over Amazonia. *J. Geophys. Res. Atmos.* **1988**, *93*, 1509–1527. [CrossRef]
46. Watson, J.G.; Chow, J.C. Source characterization of major emission sources in the Imperial and Mexicali Valleys along the US/Mexico border. *Sci. Total Environ.* **2001**, *276*, 33–47. [CrossRef] [PubMed]
47. Cachier, H.; Bremond, M.-P.; Buat-Ménard, P. Determination of atmospheric soot carbon with a simple thermal method. *Tellus B Chem. Phys. Meteorol.* **1989**, *41*, 379. [CrossRef]

48. Chow, J.C.; Watson, J.G.; Pritchett, L.C.; Pierson, W.R.; Frazier, C.A.; Purcell, R.G. The direct thermal/optical reflectance carbon analysis system: Description, evaluation and applications in U.S. Air quality studies. *Atmos. Environ. A Gen. Top.* **1993**, *27*, 1185–1201. [CrossRef]
49. Schmid, H.; Laskus, L.; Abraham, H.J.; Baltensperger, U.; Lavanchy, V.; Bizjak, M.; Burba, P.; Cachier, H.; Crow, D.; Chow, J.; et al. Results of the “carbon conference” international aerosol carbon round robin test stage I. *Atmos. Environ.* **2001**, *35*, 2111–2121. [CrossRef]
50. Hitzenger, R.; Petzold, A.; Bauer, H.; Ctyroky, P.; Pouresmaeil, P.; Laskus, L.; Puxbaum, H. Intercomparison of Thermal and Optical Measurement Methods for Elemental Carbon and Black Carbon at an Urban Location. *Environ. Sci. Technol.* **2006**, *40*, 6377–6383. [CrossRef] [PubMed]
51. Andreae, M.O. Soot Carbon and Excess Fine Potassium: Long-Range Transport of Combustion-Derived Aerosols. *Science* **1983**, *220*, 1148–1151. [CrossRef] [PubMed]
52. Cheng, Y.; Zheng, M.; He, K.-B.; Chen, Y.; Yan, B.; Russell, A.G.; Shi, W.; Jiao, Z.; Sheng, G.; Fu, J.; et al. Comparison of two thermal-optical methods for the determination of organic carbon and elemental carbon: Results from the southeastern United States. *Atmos. Environ.* **2011**, *45*, 1913–1918. [CrossRef]
53. Sciare, J.; Oikonomou, K.; Favez, O.; Liakakou, E.; Markaki, Z.; Cachier, H.; Mihalopoulos, N. Long-term measurements of carbonaceous aerosols in the Eastern Mediterranean: Evidence of long-range transport of biomass burning. *Atmos. Chem. Phys. Discuss.* **2008**, *8*, 5551–5563. Available online: <http://hal.archives-ouvertes.fr/hal-00328321/> (accessed on 1 November 2012). [CrossRef]
54. Chow, J.C.; Watson, J.G.; Chen, L.W.A.; Chang, M.C.; Paredes-Miranda, G. Comparison of the DRI/OGC and Model 2001 Thermal/Optical Carbon Analyzers. Final Report for the IMPROVE Steering Committee; Desert Research Institute: Reno, NV, USA, 2005; Available online: http://vista.cira.colostate.edu/improve/publications/GrayLit/013_CarbonAnalyzer/IMPROVECarbonAnalyzerAssessment.doc (accessed on 3 April 2023).
55. Paatero, P.; Tapper, U. Positive matrix factorization: A non-negative factor model with optimal utilization of error estimates of data values. *Environmetrics* **1994**, *5*, 111–126. [CrossRef]
56. Polissar, A.V.; Hopke, P.K.; Poirot, R.L. Atmospheric Aerosol over Vermont: Chemical Composition and Sources. *Environ. Sci. Technol.* **2001**, *35*, 4604–4621. [CrossRef] [PubMed]
57. Chan, Y.-C.; Hawas, O.; Hawker, D.; Vowles, P.; Cohen, D.D.; Stelcer, E.; Simpson, R.; Golding, G.; Christensen, E. Using multiple type composition data and wind data in PMF analysis to apportion and locate sources of air pollutants. *Atmos. Environ.* **2011**, *45*, 439–449. [CrossRef]
58. Laupsa, H.; Denby, B.; Larssen, S.; Schaug, J. Source apportionment of particulate matter (PM_{2.5}) in an urban area using dispersion, receptor and inverse modelling. *Atmos. Environ.* **2009**, *43*, 4733–4744. [CrossRef]
59. Yue, W.; Stölzel, M.; Cyrys, J.; Pitz, M.; Heinrich, J.; Kreyling, W.G.; Wichmann, H.-E.; Peters, A.; Wang, S.; Hopke, P.K. Source apportionment of ambient fine particle size distribution using positive matrix factorization in Erfurt, Germany. *Sci. Total Environ.* **2008**, *398*, 133–144. [CrossRef] [PubMed]
60. Paatero, P.; Hopke, P.K. Discarding or downweighting high-noise variables in factor analytic models. *Anal. Chim. Acta* **2003**, *490*, 277–289. [CrossRef]
61. Gupta, I.; Salunkhe, A.; Kumar, R. Source Apportionment of PM₁₀ by Positive Matrix Factorization in Urban Area of Mumbai, India. *Sci. World J.* **2012**, *2012*, 1–13. [CrossRef]
62. Draxler, R.R.; Hess, G.D. An Overview of the HYSPLIT_4 Modeling System of Trajectories, Dispersion, and Deposition. *Aust. Meteorol. Mag.* **1998**, *47*, 295–308.
63. Adon, A.J.; Liousse, C.; Doumbia, E.T.; Baeza-Squiban, A.; Cachier, H.; Léon, J.F.; Yoboué, V.; Akpo, A.B.; Galy-Lacaux, C.; Guinot, B. Physico-chemical characterization of urban aerosols from specific combustion sources in West Africa at Abidjan in Côte d’Ivoire and Cotonou in Benin in the frame of DACCIWA program. *Atmos. Chem. Phys. Discuss.* **2020**, *20*, 5327–5354. [CrossRef]
64. Kebe, M.; Traore, A.; Manousakas, M.; Vasilatou, V.; Ndao, A.; Wague, A.; Eleftheriadis, K. Source Apportionment and Assessment of Air Quality Index of PM_{2.5–10} and PM_{2.5} in at Two Different Sites in Urban Background Area in Senegal. *Atmosphere* **2021**, *12*, 182. [CrossRef]
65. Putaud, J.-P.; Raes, F.; Van Dingenen, R.; Brüggemann, E.; Facchini, M.-C.; Decesari, S.; Fuzzi, S.; Gehrig, R.; Hüglin, C.; Laj, P.; et al. A European aerosol phenomenology—2: Chemical characteristics of particulate matter at kerbside, urban, rural and background sites in Europe. *Atmos. Environ.* **2004**, *38*, 2579–2595. [CrossRef]
66. Querol, X.; Alastuey, A.; Viana, M.; Rodriguez, S.; Artiñano, B.; Salvador, P.; Santos, S.G.D.; Patier, R.F.; Ruiz, C.; de la Rosa, J.; et al. Speciation and origin of PM₁₀ and PM_{2.5} in Spain. *J. Aerosol Sci.* **2004**, *35*, 1151–1172. [CrossRef]
67. Yu, J.Z.; Tung, J.W.T.; Wu, A.W.M.; Lau, A.K.H.; Louie, P.K.-K.; Fung, J.C.H. Abundance and seasonal characteristics of elemental and organic carbon in Hong Kong PM₁₀. *Atmos. Environ.* **2004**, *38*, 1511–1521. [CrossRef]
68. McLennan, S.M. Relationships between the trace element composition of sedimentary rocks and upper continental crust. *Geochem. Geophys. Geosyst.* **2001**, *2*, 1021–1024. [CrossRef]
69. Nyanganyura, D.; Maenhaut, W.; Mathuthu, M.; Makarau, A.; Meixner, F.X. The chemical composition of tropospheric aerosols and their contributing sources to a continental background site in northern Zimbabwe from 1994 to 2000. *Atmos. Environ.* **2007**, *41*, 2644–2659. [CrossRef]

70. Zheng, M.; Salmon, L.G.; Schauer, J.J.; Zeng, L.; Kiang, C.S.; Zhang, Y.; Cass, G.R. Seasonal trends in PM_{2.5} source contributions in Beijing, China. *Atmos. Environ.* **2005**, *39*, 3967–3976. [CrossRef]
71. Guinot, B.; Cachier, H.; Sciare, J.; Tong, Y.; Xin, W.; Jianhua, Y. Beijing aerosol: Atmospheric interactions and new trends. *J. Geophys. Res. Atmos.* **2007**, *112*, D14314. [CrossRef]
72. Sandradewi, J.; Prévôt, A.S.H.; Weingartner, E.; Schmidhauser, R.; Gysel, M.; Baltensperger, U. A study of wood burning and traffic aerosols in an Alpine valley using a multi-wavelength Aethalometer. *Atmos. Environ.* **2008**, *42*, 101–112. [CrossRef]
73. Pio, C.; Cerqueira, M.; Harrison, R.M.; Nunes, T.; Mirante, F.; Alves, C.; Oliveira, C.; de la Campa, A.S.; Artíñano, B.; Matos, M. OC/EC ratio observations in Europe: Re-thinking the approach for apportionment between primary and secondary organic carbon. *Atmos. Environ.* **2011**, *45*, 6121–6132. [CrossRef]
74. Bukowiecki, N.; Lienemann, P.; Hill, M.; Furger, M.; Richard, A.; Amato, F.; Prévôt, A.; Baltensperger, U.; Buchmann, B.; Gehrig, R. PM₁₀ emission factors for non-exhaust particles generated by road traffic in an urban street canyon and along a freeway in Switzerland. *Atmos. Environ.* **2010**, *44*, 2330–2340. [CrossRef]
75. Amato, F.; Pandolfi, M.; Moreno, T.; Furger, M.; Pey, J.; Alastuey, A.; Bukowiecki, N.; Prevot, A.; Baltensperger, U.; Querol, X. Sources and variability of inhalable road dust particles in three European cities. *Atmos. Environ.* **2011**, *45*, 6777–6787. [CrossRef]
76. Sternbeck, J.; Sjödin, Å.; Andréasson, K. Metal emissions from road traffic and the influence of resuspension—Results from two tunnel studies. *Atmos. Environ.* **2002**, *36*, 4735–4744. [CrossRef]
77. Thorpe, A.; Harrison, R.M. Sources and properties of non-exhaust particulate matter from road traffic: A review. *Sci. Total Environ.* **2008**, *400*, 270–282. [CrossRef] [PubMed]
78. Adepetu, J.A.; Asubiojo, O.I.; Iskander, F.Y.; Bauer, T.L. Elemental composition of Nigerian harmattan dust. *J. Radioanal. Nucl. Chem.* **1988**, *121*, 141–147. Available online: <http://www.springerlink.com/index/T3631906PT6M2428.pdf> (accessed on 24 August 2012). [CrossRef]
79. Almeida, S.; Pio, C.; Freitas, M.; Reis, M.; Trancoso, M. Source apportionment of fine and coarse particulate matter in a sub-urban area at the Western European Coast. *Atmos. Environ.* **2005**, *39*, 3127–3138. [CrossRef]
80. Watson, J.G. Protocol for Applying and Validating the CMB Model for PM_{2.5} and VOC. US Environmental Protection Agency, Air Quality Modeling Group. *Desert Res. Inst.* **2004**. Available online: <http://purl.access.gpo.gov/GPO/LPS63500> (accessed on 3 April 2023).
81. Lioussé, C.; Galy-Lacaux, C. Urban pollution in West Africa. *La Météorol.* **2010**, *71*. Available online: <http://hdl.handle.net/2042/37377> (accessed on 15 February 2023).
82. Seinfeld, J.H.; Pandis, S. *Atmospheric Chemistry and Physics: From Air Pollution to Climate Change*, 2nd ed.; Wiley: New York, NY, USA, 2006; Available online: <https://www.wiley.com/en-ae/Atmospheric+Chemistry+and+Physics%3A+From+Air+Pollution+to+Climate+Change%2C+2nd+Edition-p-9780471720188> (accessed on 6 June 2018).
83. Pekney, N.J.; Davidson, C.I.; Robinson, A.; Zhou, L.; Hopke, P.; Eatough, D.; Rogge, W.F. Major Source Categories for PM_{2.5} in Pittsburgh using PMF and UNMIX. *Aerosol Sci. Technol.* **2006**, *40*, 910–924. [CrossRef]
84. Bhanuprasad, S.; Venkataraman, C.; Bhushan, M. Positive matrix factorization and trajectory modelling for source identification: A new look at Indian Ocean Experiment ship observations. *Atmos. Environ.* **2008**, *42*, 4836–4852. [CrossRef]
85. Goldberg, E.D. *Composition of Sea Water, Comparative Oceanography*; Hill, H.M., Ed.; Wiley: New York, NY, USA, 1963.
86. Millero, F.J.; Feistel, R.; Wright, D.G.; McDougall, T.J. The composition of Standard Seawater and the definition of the Reference-Composition Salinity Scale. *Deep Sea Res. Part I Oceanogr. Res. Pap.* **2008**, *55*, 50–72. [CrossRef]
87. Yuan, Z.; Lau, A.K.H.; Zhang, H.; Yu, J.Z.; Louie, P.K.; Fung, J.C. Identification and spatiotemporal variations of dominant PM₁₀ sources over Hong Kong. *Atmos. Environ.* **2006**, *40*, 1803–1815. [CrossRef]
88. Allen, J.O.; Mayo, P.R.; Hughes, L.S.; Salmon, L.G.; Cass, G.R. Emissions of Size-Segregated Aerosols from On-Road Vehicles in the Caldecott Tunnel. *Environ. Sci. Technol.* **2001**, *35*, 4189–4197. [CrossRef]
89. Pacyna, J.M.; Pacyna, E.G. An assessment of global and regional emissions of trace metals to the atmosphere from anthropogenic sources worldwide. *Environ. Rev.* **2001**, *9*, 269–298. [CrossRef]
90. Petaloti, C.; Triantafyllou, A.; Kouimtzi, T.; Samara, C. Trace elements in atmospheric particulate matter over a coal burning power production area of western Macedonia, Greece. *Chemosphere* **2006**, *65*, 2233–2243. [CrossRef]
91. Lee, J.H.; Kim, Y.P.; Moon, K.-C.; Kim, H.-K.; Lee, C.B. Fine particle measurements at two background sites in Korea between 1996 and 1997. *Atmos. Environ.* **2001**, *35*, 635–643. [CrossRef]
92. Cohen, D.D.; Crawford, J.; Stelcer, E.; Bac, V.T. Characterisation and source apportionment of fine particulate sources at Hanoi from 2001 to 2008. *Atmos. Environ.* **2010**, *44*, 320–328. [CrossRef]

Disclaimer/Publisher’s Note: The statements, opinions and data contained in all publications are solely those of the individual author(s) and contributor(s) and not of MDPI and/or the editor(s). MDPI and/or the editor(s) disclaim responsibility for any injury to people or property resulting from any ideas, methods, instructions or products referred to in the content.